

AUTHOR QUERY FORM

 ELSEVIER	Journal: NEUCOM Article Number: 23574	Please e-mail your responses and any corrections to: E-mail: corrections.esch@elsevier.sps.co.in
--	--	--

Dear Author,

Please check your proof carefully and mark all corrections at the appropriate place in the proof. **It is crucial that you NOT make direct edits to the PDF using the editing tools as doing so could lead us to overlook your desired changes.** Rather, please request corrections by using the tools in the Comment pane to annotate the PDF and call out the changes you would like to see. To ensure fast publication of your paper please return your corrections within 48 hours.

For correction or revision of any artwork, please consult <http://www.elsevier.com/artworkinstructions>.

Any queries or remarks that have arisen during the processing of your manuscript are listed below and highlighted by flags in the proof.

Location in article	Query / Remark: Click on the Q link to find the query's location in text Please insert your reply or correction at the corresponding line in the proof
<u>Q1</u> <u>Q2</u>	<p>Your article is registered as a regular item and is being processed for inclusion in a regular issue of the journal. If this is NOT correct and your article belongs to a Special Issue/Collection please contact n.ram@elsevier.com immediately prior to returning your corrections.</p> <p>The author names have been tagged as given names and surnames (surnames are highlighted in teal color). Please confirm if they have been identified correctly.</p>
<input type="checkbox"/>	<p>Please check this box or indicate your approval if you have no corrections to make to the PDF file</p>

Thank you for your assistance.

Highlights

-
- In-depth time complexity analysis of typical graph neural networks (GNN).
 - Experimental analysis of performance characteristics of GNN training and inference.
 - The edge-related calculation is the main performance bottleneck.
 - Efficiency of the sampling techniques for GNNs should be improved.
-

Uncorrected Proof



5

3 **q1 Empirical analysis of performance bottlenecks in graph neural network
4 training and inference with GPUs**7 **q2 Zhaokang Wang, Yunpan Wang, Chunfeng Yuan, Rong Gu^{*,1}, Yihua Huang^{*,1}**

8 State Key Laboratory for Novel Software Technology, Department of Computer Science and Technology, Nanjing University, Nanjing 210023, China

9 10 **ARTICLE INFO**

13 Article history:

14 Received 10 September 2020

15 Revised 27 February 2021

16 Accepted 3 March 2021

17 Available online xxxx

18 Communicated by Zidong Wang

19 **Keywords:**

20 Graph neural network

21 Performance bottleneck analysis

22 Empirical evaluation

23 Machine learning system

24 GPU

26 **ABSTRACT**

The graph neural network (GNN) has become a popular research area for its state-of-the-art performance in many graph analysis tasks. Recently, various graph neural network libraries have emerged. They make the development of GNNs convenient, but their performance bottlenecks on large datasets are not well studied. In this work, we analyze the performance bottlenecks in GNN training and inference with GPUs empirically. A GNN layer can be decomposed into two parts: the vertex and the edge calculation parts. According to their computational complexity, we select four representative GNNs (GCN, GGNN, GAT, GaAN) for evaluation. We decompose their running time and memory usage, evaluate the effects of hyper-parameters and assess the efficiency of the sampling techniques. The experimental evaluation with PyTorch Geometric indicates that the edge-related calculation is the performance bottleneck for most GNNs, dominating the training/inference time and memory usage. The sampling techniques are essential for GNN training and inference on big graphs with GPUs, but their current implementation still has non-trivial overheads in sampling and data transferring.

27 © 2021 Published by Elsevier B.V.

42

43 **1. Introduction**

In recent years, the graph neural network (GNN) becomes a hot research topic in the field of artificial intelligence. Many GNNs [1–7] are proposed. They can learn the representation of vertices/edges in a graph from its topology and the original feature vectors in an *end-to-end* manner. The powerful expression capability makes GNNs achieve good accuracy in not only graph analytical tasks [8–10] (like node classification and link prediction) but also computer vision tasks (like human-object interaction [11], human parsing [12], and video object segmentation [13]).

To train GNNs easily, a series of GNN libraries/systems [14–18] are proposed. PyTorch Geometric (PyG) [14], NeuGraph [16], PGL [18] and Deep Graph Library (DGL) [15] build upon the existing deep learning frameworks (PyG on PyTorch, NeuGraph on TensorFlow, PGL on PaddlePaddle, DGL on multiple backends). They provide users with a high-level programming model (the message-passing framework for PyG/PGL/DGL and the SAGA-NN model for NeuGraph) to describe the structure of a GNN. They take

44 advantage of the common tools provided by the underlying frameworks like the automatic differentiation to simplify the development. They utilize specially optimized CUDA kernels (like kernel fusion [15,16]) and other implementation techniques (like 2D graph partitioning [16]) to improve the speed of GNN training on 45 GPUs.

46 However, what is the real performance bottleneck in GNN training 47 and inference is still in doubt. Yan et al. [19] and Zhang et al. 48 [20] experimentally analyze the architectural characteristics of 49 GNN inference. They find that the GNN inference is more cache-friendly than the traditional graph analysis tasks (like PageRank 50 and is suitable for GPUs. They verify the effectiveness of the kernel 51 fusion optimization in reducing the time of inference. Nevertheless, 52 they only analyze the inference stage, ignoring the effects of 53 the backpropagation during training.

54 To explore essential performance bottlenecks in both GNN 55 training and inference, we conduct a range of experimental analysis 56 in this work. We focus on the efficiency bottlenecks of GNN 57 training and inference. We model the GNNs with the message- 58 passing framework that decomposes a GNN layer into two parts: 59 the vertex calculation and the edge calculation. According to the 60 time complexity of the two parts, we classify the typical GNNs into 61 four quadrants ({high, low} complexity × {vertex, edge} calculation). 62 We choose GCN [1], GGNN [4], GAT [6], and GaAN [7] as 63 representative GNNs of the four quadrants.

* Corresponding authors.

E-mail addresses: wangzhaokang@mail.nju.edu.cn (Z. Wang), wangyp@mail.nju.edu.cn (Y. Wang), cfyuan@nju.edu.cn (C. Yuan), gurong@nju.edu.cn (R. Gu), yhuang@nju.edu.cn (Y. Huang).

¹ Corresponding authors with equal contribution.

We implement them with PyG and evaluate their efficiency and accuracy with six real-world datasets on a GPU card. We identify the most time-consuming stage in GNN training and inference by decomposing the training and inference time per epoch from the layer level to the operator level. We also analyze the memory usage during training and inference to discover the main factor that limits the data scalability of GNN training and inference on GPUs. Finally, we evaluate whether or not the sampling techniques affect the performance bottlenecks and accuracy. The key findings and insights are summarized below.

- The training and inference time and the memory usage of a GNN layer are mainly affected by the dimensions of the input/output hidden vectors. Fixing other hyper-parameters, the training and inference time and the memory usage of a GNN layer increase linearly with the dimensions.
- The edge-related calculation is the performance bottleneck for most GNNs. For GNNs with high edge calculation complexity, most of the training and inference time is spent on conducting the messaging function for every edge. For GNNs with low edge calculation complexity, the collection and aggregation of message vectors of all edges consume most of the training and inference time.
- The high memory usage of the edge calculation stage is the main factor limiting the data scalability of GNN training and inference. The edge calculation generates (and caches) many intermediate results. They are an order of magnitude larger than the dataset itself. As GPUs have limited on-chip memory, high memory consumption prevents us from performing training and inference on big graphs.
- The sampling techniques can significantly reduce the memory usage of training and inference. The sampling techniques are essential for performing GNN training and inference on big graphs with GPUs. The accuracy of the GNN models trained with the sampling techniques is close to the accuracy of full-batch training. However, the existing implementation of sampling is still inefficient. The time spent on sampling may exceed the time spent on training and inference. Under small batch sizes, the sampled graphs are also small, wasting the computing power of GPUs.

Based on the insights, we provide several potential optimization directions:

- To reduce training and inference time, optimizations should focus on improving the efficiency of the edge calculation. One may consider developing optimized operators for the messaging step that is the major source of computing costs in the edge calculation. Fusing operators of the collection step, messaging function and the aggregation step together is another way to reduce the overheads in the edge calculation.
- To reduce memory usage, optimizations should focus on reducing the intermediate results in the edge calculation. One may consider adopting the checkpoint mechanism to cache less intermediate results during the forward phase and re-calculate the needed data on the fly during the backpropagation.
- To improve the efficiency of the sampling techniques, one may consider overlapping the sampling on the CPU side with the training/inference on the GPU side. Choosing a proper batch size automatically is another potential optimization.

We hope that our analysis can help the developers of the GNN libraries/systems have a better understanding of the characteristics of GNN training/inference and propose more targeted optimizations.

Outline. We briefly survey the typical GNNs in Section 2. We introduce our experimental setting and targets in Section 3. The experimental results are presented and analyzed in Section 4. We summarize the key findings and give out potential optimization directions in Section 5. We introduce the related work in Section 6 and conclude our work in Section 7.

2. Review of graph neural networks

In this section, we formally define the graph neural networks and briefly survey typical graph neural networks. We denote a simple undirected graph \mathcal{G} as $\mathcal{G} = (\mathcal{V}, \mathcal{E})$, where \mathcal{V} and \mathcal{E} are the vertex set and the edge set of \mathcal{G} , respectively. We use v_x ($0 \leq x < |\mathcal{V}|$) to denote a vertex and $e_{y,x} = (v_y, v_x)$ to denote the edge pointing from v_y to v_x . The adjacency set of v_x is $\mathcal{N}(v_x) = \{v | (v, v_x) \in \mathcal{E}\}$. We denote a vector with a bold lower case letter like \mathbf{h} and a matrix with a bold upper case letter like \mathbf{W} . Table 1 summarizes the common symbols used throughout this work. We use blue characters \mathbf{w}/\mathbf{W} to denote weight vectors/matrices that are model parameters to train in a GNN.

2.1. Structure of graph neural networks

As illustrated in Fig. 1, a typical GNN can be decomposed into three parts: an input layer + several GNN layers + a prediction layer.

In the input layer, A GNN receives a graph \mathcal{G} as the input. Every vertex v_x in \mathcal{G} is attached with a feature vector \mathbf{v}_x to describe the properties of the vertex. Every edge $e_{y,x}$ of \mathcal{G} may also be attached with a feature vector $\mathbf{e}_{y,x}$. The input layer of a GNN receives feature vectors from all vertices and passes the feature vectors to the first GNN layer (i.e. GNN layer 0).

A GNN usually consists of more than one GNN layer. Each GNN layer consists of $|\mathcal{V}|$ graph neurons, where $|\mathcal{V}|$ is the number of vertices in \mathcal{G} . Each graph neuron corresponds to a vertex in \mathcal{G} . Different GNNs mainly differ in the graph neurons that they use. We elaborate on the details of graph neurons later. GNN layers are sparsely connected with the input layer and other GNN layers.

- In the first GNN layer (layer 0), a graph neuron collects feature vectors from the input layer. For the graph neuron corresponding to the vertex v_x , it collects the feature vector \mathbf{v}_x and the feature vectors \mathbf{v}_y of the vertices v_y that are adjacent to v_x (i.e. $v_y \in \mathcal{N}(v_x)$). The graph neuron aggregates input feature vectors, apply non-linear transformation, and outputs a hidden vector \mathbf{h}_x^1 for v_x . Take the demo GNN in Fig. 1a as an example. Since $\mathcal{N}(v_3) = \{v_1, v_2, v_4, v_5, v_6\}$, the graph neuron of v_3 at the GNN layer 0 collects the input feature vectors $\{\mathbf{v}_1, \mathbf{v}_2, \mathbf{v}_3, \mathbf{v}_4, \mathbf{v}_5, \mathbf{v}_6\}$ from the input layer and outputs \mathbf{h}_3^1 . The connections between the first GNN layer and the input layer are determined by the topology of \mathcal{G} . The graph neuron of v_x in the first GNN layer is connected with the input unit of v_y in the input layer only if there is an edge $e_{y,x}$ between v_y and v_x in \mathcal{G} . Since most real-world graphs are very sparse (i.e. $|\mathcal{E}| \ll |\mathcal{V}|^2$), the connections between the first GNN layer and the input layer are also sparse, different from the traditional neural networks.
- In the next GNN layer (layer 1), the graph neuron corresponding to v_x collects the hidden vector of itself \mathbf{h}_x^1 and its adjacent vertices (\mathbf{h}_y^1 with $v_y \in \mathcal{N}(v_x)$) from the previous GNN layer. Thus, the connections between the first and the second GNN layers are also determined by the topology of \mathcal{G} . Based on the collected hidden vectors, the graph neuron in the layer 1 outputs a new hidden vector \mathbf{h}_x^2 for v_x .

Table 1

Frequently-used symbols.

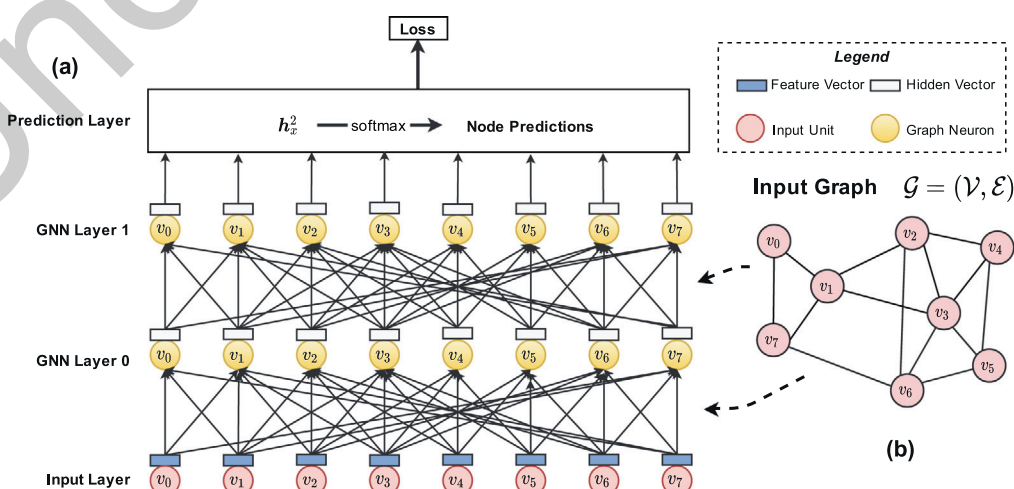
Category	Symbol	Meaning
Graph Structure	$\mathcal{G} = (\mathcal{V}, \mathcal{E})$	The simple undirected input graph with the vertex set \mathcal{V} and the edge set \mathcal{E} .
	v_x	The x -th vertex of the input graph.
	$e_{y,x}$	The edge pointing from v_y to v_x of the input graph.
	$\mathcal{N}(v_x)$	The adjacency set of v_x in the input graph.
	\bar{d}	The average degree of the input graph.
GNN Definition	L	The number of GNN layers.
	K	The number of heads in a GNN layer.
	ϕ^l	The messaging function of the GNN layer l .
	Σ^l	The aggregation function of the GNN layer l .
	γ^l	The vertex updating function of the GNN layer l .
	$\phi^{l,i} / \Sigma^{l,i} / \gamma^{l,i}$	The messaging/aggregation/updating function of the i -th sub-layer of the GNN layer l .
	$\mathbf{W}^l, \mathbf{W}^{(k)}/\mathbf{b}, \mathbf{a}$	The matrices/vectors represented by the blue characters are the weight matrices/vectors that need to be learned in the GNN.
Vector	\mathbf{v}_x	The feature vector of the vertex v_x .
	$\mathbf{e}_{y,x}$	The feature vector of the edge $e_{y,x}$.
	\mathbf{h}_x^l	The input hidden vector of the graph neuron corresponding to v_x in the GNN layer l .
	\mathbf{h}_x^{l+1}	The output hidden vector of the graph neuron corresponding to v_x in the GNN layer l .
	$\mathbf{m}_{y,x}^l$	The message vector of the edge $e_{y,x}$ outputted by ϕ^l of the GNN layer l .
	\mathbf{s}_x^l	The aggregated vector of the vertex v_x outputted by Σ^l of the GNN layer l .
	$\mathbf{h}_x^{l,i}/\mathbf{m}_{y,x}^l/\mathbf{s}_x^l$	The hidden/message/aggregated vector of the vertex v_x outputted by $\gamma^{l,i}/\phi^{l,i}/\Sigma^{l,i}$ of the i -th sub-layer of the GNN layer l .
	d_{in}^l, d_{out}^l	The dimension of the input/output hidden vectors of the GNN layer l .
	$\dim(\mathbf{x})$	The dimension of a vector \mathbf{x} .

- 206 • A GNN allows stacking more GNN layers to support deeper
207 graph analysis. Assume there are L GNN layers in total. The last
208 GNN layer ($layer L - 1$) outputs a hidden vector \mathbf{h}_x^L for every vertex
209 v_x . \mathbf{h}_x^L is an embedding vector that encodes the knowledge
210 learned from the input layer and all the previous GNN layers.
211 Since \mathbf{h}_x^L is affected by v_x and the vertices in the L -hop neighbor-
212 hood of v_x , analyzing a graph with more GNN layers means ana-
213 lyzing each vertex with a wider scope. The hidden vectors \mathbf{h}_x^L of
214 the last GNN layer are fed to the prediction layer to generate the
215 output for the whole GNN.

216 The prediction layer is a standard neural network. The structure
217 of the prediction layer depends on the prediction task of the GNN.
218 Take the node classification task in Fig. 1 as the example. The node
219 classification predicts a label for every vertex in \mathcal{G} . In this case, the
220 prediction layer can be a simple softmax layer with \mathbf{h}_x^L as the input
221

and a vector of probabilities as the output. If the prediction task is
222 the edge prediction, the hidden vectors of two vertices are concate-
223 nated and fed into a softmax layer. If we need to predict a label for
224 the whole graph, a pooling (max/mean/...) layer is added to gener-
225 ate an embedding vector for the whole graph and the embedding
226 vector is used to produce the final prediction.

227 Supporting end-to-end training is a prominent advantage of
228 GNNs, compared with traditional graph-based machine learning
229 methods. The traditional methods need to construct input feature
230 vectors for vertices and edges manually or use embedding methods
231 like DeepWalk [21] and node2vec [22]. The feature vector genera-
232 tion is independent of model training. Therefore, generated feature
233 vectors may not be suitable for downstream prediction tasks. In
234 GNNs, gradients are propagated from the prediction layer back to
235 GNN layers layer by layer. The model parameters in the GNN layers
236 are updated based on the feedback from the downstream predic-
237 tion task. In a fully parameterized way, a GNN can automatically
238

**Fig. 1.** Structure of a typical graph neural network. (a) Demo GNN, (b) Demo graph. The target application is the node classification. The demo GNN has two GNN layers.

239 extract an embedding vector for each vertex from its L -hop neighborhood, tuned according to the specific prediction task.
 240

241 2.2. Graph neuron and message-passing framework

242 Graph neurons are building blocks of a GNN. A GNN layer consists of $|\mathcal{V}|$ graph neurons. Each vertex corresponds to a graph neuron.
 243 A graph neuron is a small neural network. For the graph neuron corresponding to v_x at the layer l , it receives the hidden
 244 vector of itself \mathbf{h}_x^l and the hidden vectors of its adjacent vertices
 245 \mathbf{h}_y^l with $v_y \in \mathcal{N}(v_x)$ from the previous GNN layer.² The graph neuron
 246 of v_x aggregates the received hidden vectors, applies non-
 247 linear transformations, and outputs a new hidden vector \mathbf{h}_x^{l+1} .
 248

249 We follow the message-passing framework [23] to formally
 250 define a graph neuron. The message-passing framework is widely
 251 used in the cutting-edge GNN libraries like PyG [14] and DGL
 252 [15]. Fig. 2 shows the internal structure of a graph neuron in the
 253 message-passing framework. A graph neuron at the layer l are
 254 made of three *differentiable* functions: the messaging function ϕ^l ,
 255 the aggregation function Σ^l , and the updating function γ^l .
 256

257 The graph neuron of v_x calculates the output hidden vector \mathbf{h}_x^{l+1}
 258 with the three functions in three steps:

- 259 1. For every adjacent edge (v_y, v_x) of v_x ($v_y \in \mathcal{N}(v_x)$), the messag-
 260 ing function ϕ^l receives the output hidden vectors \mathbf{h}_y^l and \mathbf{h}_x^l
 261 from the previous GNN layer and the edge feature vector $\mathbf{e}_{y,x}$
 262 (and other feature vectors associated with v_x/v_y if necessary)
 263 as the input. ϕ^l emits a *message vector* $\mathbf{m}_{y,x}^l$ for every edge
 264 (v_y, v_x) at the layer l , i.e. $\mathbf{m}_{y,x}^l = \phi^l(\mathbf{h}_y^l, \mathbf{h}_x^l, \mathbf{e}_{y,x}, \dots)$;
 265 2. The aggregation function Σ^l then aggregates the message vectors
 266 $\mathbf{m}_{y,x}^l$ of the adjacent edges $(v_y \in \mathcal{N}(v_x))$ to produce an *aggre-*
 267 *gated vector* \mathbf{s}_x^l , i.e. $\mathbf{s}_x^l = \sum_{v_y \in \mathcal{N}(v_x)}^l \mathbf{m}_{y,x}^l$;
 268 3. The updating function γ^l calculates the hidden vector of this
 269 layer \mathbf{h}_x^{l+1} based on the hidden vector from the previous layer
 270 \mathbf{h}_x^l and the aggregated vector \mathbf{s}_x^l (and other feature vectors asso-
 271 ciated with v_x if necessary), i.e. $\mathbf{h}_x^{l+1} = \gamma^l(\mathbf{h}_x^l, \mathbf{s}_x^l, \dots)$.
 272

273 Briefly, the behaviour of a graph neuron under the message-
 274 passing framework can be defined as
 275

$$276 \mathbf{h}_x^{l+1} = \gamma^l(\mathbf{h}_x^l, \Sigma_{v_y \in \mathcal{N}(v_x)}^l \phi^l(\mathbf{h}_y^l, \mathbf{h}_x^l, \mathbf{e}_{y,x}, \dots), \dots). \quad (1)$$

277 The end-to-end training requires ϕ^l and γ^l (like multi-layer per-
 278 ceptrons and GRUs) and Σ^l (like mean, sum, element-wise min/-
 279 max) are *differentiable* to make the whole GNN differentiable.
 280

281 Different GNNs have different definitions of the three functions.
 282 We regard ϕ and Σ as *edge calculation* functions, since they are con-
 283 ducted over every edge in \mathcal{G} . We regard γ as the *vertex calculation*
 284 function, as it is conducted over every vertex in \mathcal{G} . Table 2 and
 285 Table 3 list the edge calculation functions and the vertex calcula-
 286 tion functions of typical GNNs, respectively. Some complex GNNs
 287 like GAT [6] and GaAN [7] use more than one message passing
 288 phase in each GNN layer. We regard every message passing phase
 289 in a GNN layer as a *sub-layer*. We will give out more details on sub-
 290 layers when we introduce GAT.

291 2.3. Representative GNNs

292 We use $O_\phi/O_\Sigma/O_\gamma$ to denote the time complexity of the three
 293 functions in the message-passing framework. The time complexity

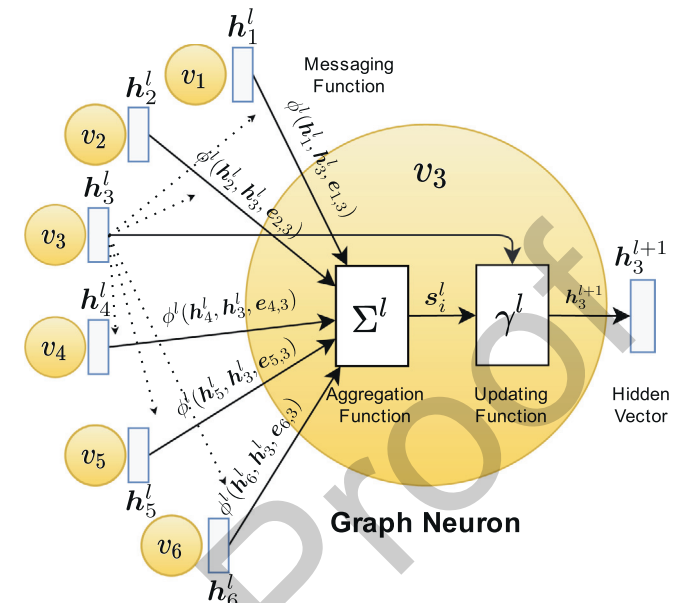


Fig. 2. Graph neuron of v_3 in the GNN layer l with the demo graph \mathcal{G} in Fig. 1b. $\phi^l/\Sigma^l/\gamma^l$ are the messaging/aggregation/updating functions in the message-passing framework.

294 of a GNN layer is made up of two parts: the edge calculation com-
 295 plexity $O_\phi + O_\Sigma$ and the vertex calculation complexity O_γ . In Table 2
 296 and Table 3, we list the edge and vertex calculation complexity of
 297 each GNN, respectively. The time complexity of a graph neuron is
 298 affected by the dimensions of the input/output hidden vectors d_h
 299 and d_{out} and the dimensions of the model parameters (like the
 300 number of heads K in GAT and the dimensions of the view vectors
 301 $d_a/d_v/d_m$ in GaAN).

302 Since we focus on analyzing the performance bottleneck in
 303 training GNNs, we classify the typical GNNs into four quadrants
 304 based on their edge/vertex complexity as shown in Fig. 3. We pick
 305 GCN, GGNN, GAT, and GaAN as the *representative* GNNs of the four
 306 quadrants.

307 2.3.1. GCN (Low vertex & low edge complexity)

308 Graph convolution network (GCN [1]) introduces the first-order
 309 approximation of the spectral-based graph convolutions into graph
 310 neural networks. It has only one parameter to learn at each layer,
 311 i.e. the weight matrix \mathbf{W}^l in the updating function γ^l . A GCN graph
 312 neuron can be expressed as $\mathbf{h}_x^{l+1} = \mathbf{W}^l \sum_{v_y \in \mathcal{N}(v_x)} w_{y,x} \mathbf{h}_y^l$, where $w_{y,x}$ is
 313 the normalized weight of the edge $e_{y,x}$. According to the associative
 314 law of the matrix multiplication, $\mathbf{h}_x^{l+1} = \sum_{v_y \in \mathcal{N}(v_x)} w_{y,x} \mathbf{W}^l \mathbf{h}_y^l$. Since
 315 the dimension of \mathbf{h}_x^{l+1} is usually smaller than \mathbf{h}_x^l in practical GCNs,
 316 the implementation of GCN in PyG chooses to first conduct the ver-
 317 tex calculation $\hat{\mathbf{h}}_y^l = \mathbf{W}^l \mathbf{h}_y^l$ for each vertex v_y and then conduct the
 318 edge calculation $\mathbf{h}_x^{l+1} = \sum_{v_y \in \mathcal{N}(v_x)} w_{y,x} \hat{\mathbf{h}}_y^l$. As $\hat{\mathbf{h}}_y^l$ has the same dimen-
 319 sion as \mathbf{h}_x^{l+1} , the implementation significantly reduces the compu-
 320 tation cost of the edge calculation.

321 2.3.2. GGNN (High vertex & low edge complexity)

322 GGNN [4] introduces the gated recurrent unit (GRU) into graph
 323 neural networks. The updating function γ^l of GGNN is a modified
 324 GRU unit that has 12 model parameters to learn, having high com-
 325 putational complexity. To lower the training cost, all GNN layers
 326 share the same group of parameters in GGNN. GGNN further
 327 requires the dimension of \mathbf{h}_x^{l+1} is equal to the dimension of \mathbf{h}^l . Since

² For the GNN layer 0, graph neurons receive input feature vectors, i.e., $\mathbf{h}_x^0 = \mathbf{v}_x$

Table 2

Typical graph neural networks and their edge calculation functions. d_{in} and d_{out} are the dimensions of the input and output hidden vectors, respectively. Blue variables are model parameters to learn. δ is the activation function.

GNN	Type	Σ^l	$\phi^l(\mathbf{h}_y^l, \mathbf{h}_x^l, \mathbf{e}_{y,x}, \dots)$	Complexity
ChebNet [2]	Spectral	sum	$\mathbf{m}_{y,x}^l = \mathbf{e}_{y,x} \mathbf{h}_y^l$	$O(d_{in})$
GCN [1]	Spectral	sum	$\mathbf{m}_{y,x}^l = \mathbf{e}_{y,x} \mathbf{h}_y^l$	$O(d_{in})$
AGCN [3]	Spectral	sum	$\mathbf{m}_{y,x}^l = \hat{\mathbf{e}}_{y,x} \mathbf{h}_y^l$	$O(d_{in})$
GraphSAGE [5]	Non-spectral	mean/LSTM	$\mathbf{m}_{y,x}^l = \mathbf{h}_y^l$	$O(1)$
GraphSAGE-pool [5]	Non-spectral	max	$\mathbf{m}_{y,x}^l = \delta(\mathbf{W}_{pool}^l \mathbf{h}_y^l + \mathbf{b}^l)$	$O(d_{in} * d_{out})$
Neural FPs [24]	Non-spectral	sum	$\mathbf{m}_{y,x}^l = \mathbf{h}_y^l$	$O(1)$
SSE [25]	Recurrent	sum	$\mathbf{m}_{y,x}^l = \mathbf{v}_y \mathbf{h}_y^l$	$O(f + d_{in})$
GGNN [4]	Gated	sum	$\mathbf{m}_{y,x}^l = \hat{\mathbf{h}}_y^l$	$O(1)$
GAT [6]	Attention	sum	Sub-layer 0 : $\mathbf{m}_{y,x}^{l,0} = \prod_{k=1}^K \exp(\text{LeakyReLU}(\mathbf{a}^T [\mathbf{h}_y[k] \hat{\mathbf{h}}_x[k]]))$ Sub-layer 1(multi-head concatenation) : $\mathbf{m}_{y,x}^{l,1} = \prod_{k=1}^K \frac{\exp(\text{LeakyReLU}(\mathbf{a}^T [\mathbf{h}_y[k] \hat{\mathbf{h}}_x[k]])))}{\hat{\mathbf{h}}_x^{l,0}[k]} \hat{\mathbf{h}}_y[k]$ Sub-layer 1(multi-head average) : $\mathbf{m}_{y,x}^{l,1} = \frac{1}{K} \sum_{k=1}^K \frac{\exp(\text{LeakyReLU}(\mathbf{a}^T [\mathbf{h}_y[k] \hat{\mathbf{h}}_x[k]])))}{\hat{\mathbf{h}}_x^{l,0}[k]} \hat{\mathbf{h}}_y[k]$	concat : $O(d_{out})$ average : $O(K * d_{out})$ Two Sub-layers
GaAN [7]	Attention	Sub-layer 0: sum Sub-layer 1: sum Sub-layer 2: max Sub-layer 3: mean	Sub-layer 0 : $\mathbf{m}_{y,x}^{l,0} = \prod_{k=1}^K \exp((\mathbf{W}_{(k),1}^l \mathbf{h}_y^l + \mathbf{b}_{(k),1}^l)^T (\mathbf{W}_{(k),2}^l \mathbf{h}_x^l + \mathbf{b}_{(k),2}^l))$ Sub-layer 1 : $\alpha_{(k)} = \frac{\exp((\mathbf{W}_{(k),1}^l \mathbf{h}_y^l + \mathbf{b}_{(k),1}^l)^T (\mathbf{W}_{(k),2}^l \mathbf{h}_x^l + \mathbf{b}_{(k),2}^l))}{\hat{\mathbf{h}}_x^{l,0}[k]}$ $\mathbf{m}_{y,x}^{l,1} = \prod_{k=1}^K \alpha_{(k)} \text{LeakyReLU}(\mathbf{W}_{(k),v}^l \mathbf{h}_y^l + \mathbf{b}_{(k),v}^l)$ Sub-layer 2 : $\mathbf{m}_{y,x}^{l,2} = \mathbf{W}_m^l \mathbf{h}_y^l + \mathbf{b}_m^l$ Sub-layer 3 : $\mathbf{m}_{y,x}^{l,3} = \mathbf{h}_y^l$	$O(\max(d_a, d_v, d_m) * K * d_{in})$ Four Sub-layers $\mathbf{W}_{(k),1}^l \in \mathbb{R}^{d_a \times d_{in}}$ $\mathbf{W}_{(k),v}^l \in \mathbb{R}^{d_v \times d_{in}}$ $\mathbf{W}_m^l \in \mathbb{R}^{d_m \times d_{in}}$

Table 3

Typical graph neural networks and their vertex calculation functions. d_{in} and d_{out} are the dimensions of the input and output hidden vectors, respectively. Blue variables are model parameters to learn. In Neural FPs, $\mathbf{W}^{l,|\mathcal{N}(i)|}$ is the weight matrix for vertices with degree $|\mathcal{N}(i)|$ at the layer l . δ is the activation function.

GNN	$\gamma^l(\mathbf{h}_x^l, \mathbf{s}_x^l, \dots)$	Complexity
ChebNet [2]	$\mathbf{h}_x^{l+1} = 2\mathbf{s}_x^l - \mathbf{h}_x^{l-1}$	$O(d_{out})$
GCN [1]	$\mathbf{h}_x^{l+1} = \mathbf{W}^l \mathbf{s}_x^l$	$O(d_{in} * d_{out})$
AGCN [3]	$\mathbf{h}_x^{l+1} = \mathbf{W}^l \mathbf{s}_x^l$	$O(d_{in} * d_{out})$
GraphSAGE [5]	$\mathbf{h}_x^{l+1} = \delta(\mathbf{W}^l [\mathbf{s}_x^l \mathbf{h}_x^l])$	$O(d_{in} * d_{out})$
GraphSAGE-pool [5]	$\mathbf{h}_x^{l+1} = \mathbf{s}_x^l$	$O(1)$
Neural FPs [24]	$\mathbf{h}_x^{l+1} = \delta(\mathbf{W}^{l, \mathcal{N}(v) } (\mathbf{t}_x^l + \mathbf{s}_x^l))$	$O(d_{in} * d_{out})$
SSE [25]	$\mathbf{h}_x^{l+1} = (1 - \alpha) \mathbf{h}_x^l + \alpha \delta(\mathbf{W}_1^l \delta(\mathbf{W}_2^l [\mathbf{v}_x \mathbf{s}_x^l]))$	$O((f + d_{in}) * d_{out})$
GGNN [4]	Preprocessing : $\hat{\mathbf{h}}_x^l = \mathbf{W}^l \mathbf{h}_x^l$ $\mathbf{z}_x^l = \delta(\mathbf{W}^l \mathbf{s}_x^l + \mathbf{b}^{sz} + \mathbf{U}^l \mathbf{h}_x^l + \mathbf{b}^{hz})$ $\mathbf{r}_x^l = \delta(\mathbf{W}^l \mathbf{s}_x^l + \mathbf{b}^{sr} + \mathbf{U}^l \mathbf{h}_x^l + \mathbf{b}^{hr})$ $\mathbf{h}_x^{l+1} = \tanh(\mathbf{W}^l \mathbf{s}_x^l + \mathbf{b}^s + \mathbf{U}^l (\odot \mathbf{h}_x^l) + \mathbf{b}^h)$ $\mathbf{h}_x^{l+1} = (1 - \mathbf{z}_x^l) \odot \mathbf{h}_x^l + \mathbf{z}_x^l \odot \hat{\mathbf{h}}_x^{l+1}$	$O(d_{in} * d_{out})$
GAT [6]	Preprocessing : $\hat{\mathbf{h}}_x^l = \prod_{k=1}^K \mathbf{W}_{(k)}^l \mathbf{h}_x^l$ Sub-layer 0 : $\mathbf{h}_x^{l,0} = \mathbf{s}_x^{l,0}$ Sub-layer 1 : $\mathbf{h}_x^{l,1} = \hat{\mathbf{h}}_x^l = \delta(\mathbf{s}_x^{l,1})$ Sub-layer 0/1/2 : $\mathbf{h}_x^{l,*} = \mathbf{s}_x^{l,*}$ Sub-layer 3 : $\mathbf{g}_x^l = \mathbf{W}_g^l [\mathbf{h}_x^l \mathbf{h}_x^{l,2} \mathbf{s}_x^{l,3}] + \mathbf{b}_g^l$ $\mathbf{h}_x^{l+1} = \mathbf{h}_x^{l,3} = \mathbf{W}_o^l [\mathbf{h}_x^l] (\mathbf{g}_x^l \odot \mathbf{h}_x^{l,1}) + \mathbf{b}_o^l$	concat : $O(d_{in} * d_{out})$ average : $O(K * d_{in} * d_{out})$ Two Sub-layers
GaAN [7]		$O(\max(K * d_v + d_{in}, 2 * d_{in} + d_m) * d_{out})$ Four Sub-layers

the messaging function ϕ^l only uses the hidden vector \mathbf{h}_y^l of the source vertex v_y for an edge $e_{y,x}$, in the implementation of PyG, GGNN conducts the pre-processing vertex calculation $\hat{\mathbf{h}}_x^l = \mathbf{W}^l \mathbf{h}_x^l$ for every vertex v_x before the message passing. The messaging function ϕ^l directly uses $\hat{\mathbf{h}}_y^l$ as the message vector for every edge $e_{y,x}$. In this way, GGNN further reduces the time complexity of

the edge calculation to $O(1)$ without increasing the time complexity of the vertex calculation.

2.3.3. GAT (Low vertex & high edge complexity)

GAT [6] introduces the multi-head attention mechanism into graph neural networks. Each GAT layer has K heads that generate

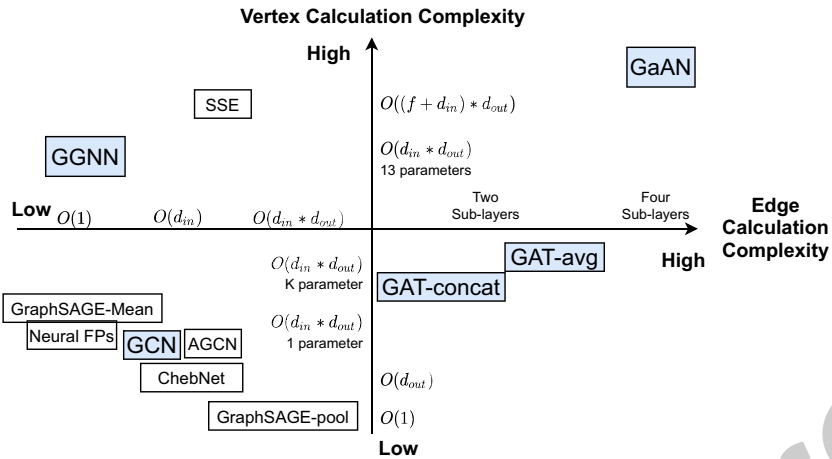


Fig. 3. Complexity quadrants of typical GNNs. We compare the complexity according to the number of sub-layers, the Big-O notation, and the number of parameters to train.

K independent views for an edge, where *K* is a hyper-parameter. The views of *K* heads can be merged by concatenating or by averaging. For concatenating, the dimension of the hidden vector of each head d_{head} is d_{out}/K . For averaging, d_{head} is d_{out} .

Each GAT layer consists of a vertex pre-processing phase and two sub-layers (i.e., message-passing phases).

The vertex pre-processing phase calculates the attention vector $\hat{\mathbf{h}}_x^l$ for every vertex v_x by $\hat{\mathbf{h}}_x = \sum_{k=1}^K \mathbf{W}_{(k)}^l \mathbf{h}_x^l$. We denote the attention sub-vector generated by the *k*-th head as $\hat{\mathbf{h}}_x[k] = \mathbf{W}_{(k)}^l \mathbf{h}_x^l$.

The first sub-layer of GAT (defined in Eq. (2)) uses the attention vectors to emit the attention weight vector $\mathbf{m}_{y,x}^{l,0}$ for every edge $e_{y,x}$ and aggregates the attention weight vectors for every vertex v_x to get the weight sum vector $\mathbf{s}_x^{l,0}$.

$$\begin{aligned} \mathbf{m}_{y,x}^{l,0} &= \phi^{l,0}(\mathbf{h}_y^l, \mathbf{h}_x^l, \mathbf{e}_{y,x}, \hat{\mathbf{h}}_y, \hat{\mathbf{h}}_x) = \sum_{k=1}^K \exp(\text{LeakyReLU}(\mathbf{a}^T [\hat{\mathbf{h}}_y[k] || \hat{\mathbf{h}}_x[k]])), \\ \mathbf{s}_x^{l,0} &= \sum_{v_y \in \mathcal{N}(v_x)} \mathbf{m}_{y,x}^{l,0}, \\ \mathbf{h}_x^{l,0} &= \gamma^{l,0}(\mathbf{h}_x^l, \mathbf{s}_x^{l,0}) = \mathbf{s}_x^{l,0}. \end{aligned} \quad (2)$$

The second sub-layer of GAT (defined in Eq. (3)) uses the weight sum vectors to normalize the attention weights for every edge and aggregates the attention vectors $\hat{\mathbf{h}}_y^l$ with the normalized weights. The aggregated attention vectors $\mathbf{s}_x^{l,1}$ are transformed by an activation function δ and are outputted as the hidden vectors of the current layer \mathbf{h}_x^{l+1} .

$$\begin{aligned} \mathbf{m}_{y,x}^{l,1} &= \phi^{l,1}(\mathbf{h}_y^{l,0}, \mathbf{h}_x^{l,0}, \mathbf{e}_{y,x}, \hat{\mathbf{h}}_y, \hat{\mathbf{h}}_x) = \sum_{k=1}^K \frac{\exp(\text{LeakyReLU}(\mathbf{a}^T [\hat{\mathbf{h}}_y[k] || \hat{\mathbf{h}}_x[k]])))}{\mathbf{s}_x^{l,0}[k]} \hat{\mathbf{h}}_y[k], \\ \mathbf{s}_x^{l,1} &= \sum_{v_y \in \mathcal{N}(v_x)} \mathbf{m}_{y,x}^{l,1}, \\ \mathbf{h}_x^{l+1} &= \mathbf{h}_x^{l,1} = \gamma^{l,1}(\mathbf{h}_x^{l,0}, \mathbf{s}_x^{l,1}) = \delta(\mathbf{s}_x^{l,1}). \end{aligned} \quad (3)$$

2.3.4. GaAN (High vertex & high edge complexity)

Based on the multi-head mechanism, GaAN [7] introduces a convolutional subnetwork to control the weight of each head. Each GaAN layer consists of four sub-layers (as defined in Table 2 and Table 3). The first two sub-layers are similar to GAT, and the last two sub-layers build the convolutional subnetwork. The first sub-layer aims to get the sum of attention weights of every vertex in all heads $\mathbf{h}_x^{l,0}$. The second sub-layer aggregates the hidden vectors from the previous GaAN layer with the normalized attention weights for all heads $\alpha_{(k)}$. The third and fourth sub-layers aggregate

the hidden vectors from the GaAN previous layer with the element-wise max and mean operators separately. The vertex updating function $\gamma^{l,3}$ of the fourth sub-layer uses the hidden vectors of the last two sub-layers $\mathbf{h}_x^{l,1}, \mathbf{h}_x^{l,2}$ to generate the output hidden vector \mathbf{h}_x^{l+1} .

2.4. Sampling techniques

By default, GNNs are trained in a full-batch way, using the whole graph in each iteration. But the full-batch gradient descent has two disadvantages [26]: (1) it has to cache intermediate results of all vertices in the forward phase, consuming lots of memory space, which is not scalable; (2) it updates the model parameters only once for each epoch, slowing the convergence of gradient descent.

To train GNNs in a mini-batch way, the sampling techniques [5,27–30,26,31] are proposed. In each mini-batch, they sample a small subgraph from the whole graph \mathcal{G} and uses the subgraph to update the model parameters. The sampling techniques only activate the graph neurons and the connections that appear in the sampled subgraph between GNN layers, as shown in Fig. 4. Inactive graph neurons and connections do not participate in the training of this mini-batch, saving lots of computation and storage costs. Moreover, it may reduce the risk of overfitting the training graph. The existing sampling techniques can be classified into two groups: *neighbor sampling* and *graph sampling*, based on whether different GNN layers sample different subgraphs.

The neighbor sampling techniques [5,27–29,32] sample nodes or edges layer by layer. The sampled subgraphs of different GNN layers may be *different*, as shown in Fig. 4(a). GraphSAGE [5] is a representative neighbor sampling technique. The technique first samples several vertices from \mathcal{V} in the last GNN layer. Then it repeatedly samples the neighbors of the sampled vertices from the previous layer until the input layer. For every sampled vertex v_x in the GNN layer l , GraphSAGE samples at most η^l neighbors of v_x from the previous layer. η^l is the hyper-parameter that is usually small. In this way, GraphSAGE limits neighborhood sizes of vertices in the sampled subgraph, especially high-degree vertices.

The graph sampling techniques [30,26,31] sample a subgraph for each mini-batch and use the same sampled subgraph for all GNN layers, as shown in Fig. 4(b). They differ in how to sample subgraphs. The cluster sampler technique [26] is a representative graph sampling technique. Given a training graph \mathcal{G} , it partitions \mathcal{G} into several dense clusters. For each mini-batch, it randomly

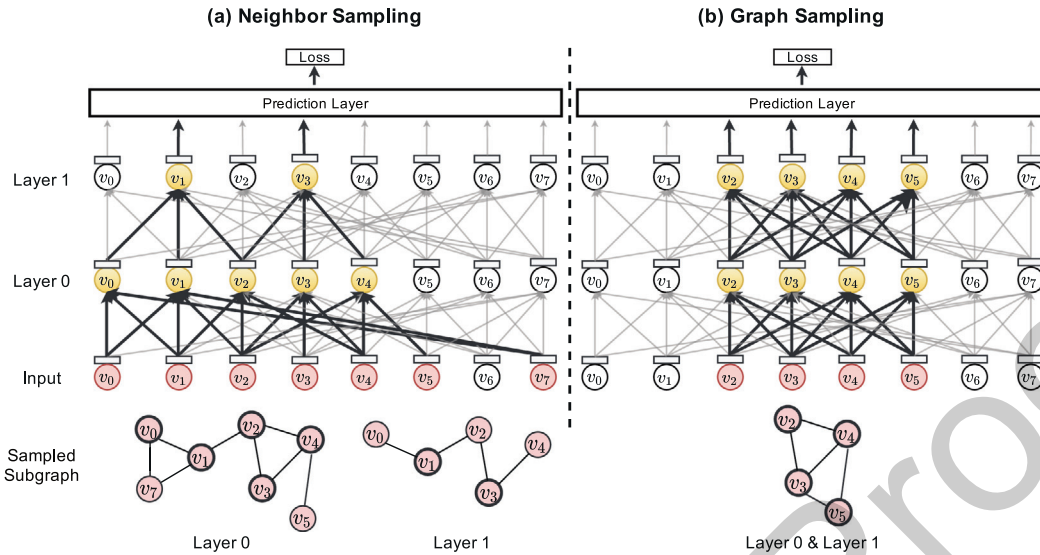


Fig. 4. Training a GNN with sampling techniques. The faded graph neurons and their connections are inactivated.

416 picks N clusters to form the sampled subgraph, where N is the
417 hyper-parameter.

418 In the implementation in PyG, the model parameters of GNNs
419 reside on the GPU side and the input graph resides on the host side.
420 To process an epoch, PyG samples the original graph in the main
421 memory and generates several batches for the epoch. For each
422 batch, PyG sends the sampled subgraph to the GPU, propagates
423 the feature vectors of the sampled subgraph from the input layer
424 to the prediction layer, calculates the gradients on the subgraph,
425 and updates the model parameters based on the gradients directly
426 on the GPU. With the sampling techniques, the model parameters
427 are updated by a stochastic gradient descent optimizer. PyG con-
428 ducts the evaluation phase every several epochs or batches (either
429 on the CPU side or the GPU side) to determine whether to stop the
430 training.

431 2.5. Inference with GNNs

432 The model parameters of a GNN consist of the weight vectors/-
433 matrices in the prediction layer and the messaging/aggregation/u-
434 pdating functions of each GNN layer. For transductive learning,
435 the input graphs of training and inference are the same. The struc-
436 ture of the GNN does not need to adjust. For inductive learning, the
437 input graphs used in training and inference are different. When we
438 want to perform inference on a new graph with a pre-trained GNN,
439 the structure of the GNN needs to be adjusted, but the hyper-
440 parameters and the model parameters of the GNN remain
441 unchanged. The number of graph neurons in each GNN layer has
442 to be adjusted to $|\mathcal{V}|$ of the new graph. The connections of graph
443 neurons between GNN layers are also adjusted according to the
444 edge set of the new graph. During inference, input feature vectors
445 of the input graph are propagated forward from the input layer to
446 the prediction layer to give out predicted labels.

447 When the memory capacity of the GPU is large enough to hold
448 all of the input graph and intermediate results during inference,
449 the inference can produce predicted labels for all vertices and
450 edges at once, making full use of the computing power of the
451 GPU. When the memory capacity is not large enough, the sampling
452 technique must be adopted.

453 The sample-based inference splits the test set into several
454 batches. For each batch, the sample-based inference samples a sub-
455 graph related to the batch from the input graph. It performs infer-

456 ence on the sampled subgraph to produce predicted labels for the
457 batch. Since the sampled subgraph is usually much smaller than
458 the original input graph, the memory usage during inference is
459 limited. The sampling method depends on the prediction task. Tak-
460 ing the node classification task as an example, if there are L GNN
461 layers in the GNN, the hidden vector outputted by the last GNN
462 layer of each vertex \mathbf{H}_x^L is only related to the L -hop neighborhood
463 of v_x . Thus, if we want to predict labels for a group of vertices,
464 we only need to sample a subgraph that contains L -hop neighbor-
465 hoods of all given vertices.

466 The implementation of sample-based inference in PyG stores
467 the whole input graph and its feature vectors in the main memory.
468 In the node classification task, it splits the vertices in the test set
469 into batches according to the given batch size. The subgraph corre-
470 sponding to each batch is sampled on the CPU side and sent to the
471 GPU side to perform inference.

472 3. Evaluation design

473 We design a series of experiments to explore the performance
474 bottleneck in training graph neural networks. We first introduce
475 our experimental setting in Section 3.1 and then give out our
476 experimental scheme in Section 3.2. The evaluation results are pre-
477 sented and analyzed later in Section 4.

478 3.1. Experimental setting

479 **Experimental Environment.** All the experiments were conducted
480 in a CentOS 7 server with the Linux kernel version 3.10.0. The ser-
481 ver had 40 cores and 90 GB main memory. The server was
482 equipped with an NVIDIA Tesla T4 GPU card with 16 GB GDDR6
483 memory. For the software environment, we adopted Python
484 3.7.7, PyTorch 1.5.0, and CUDA 10.1. We implemented all GNNs
485 with PyG 1.5.0.³

486 **Learning Task.** We used the node classification as the target task
487 in GNNs due to its popularity in real-world applications. We
488 trained GNNs in the semi-supervised learning setting. All vertices
489 and their input feature vectors were used, but only a part of the
490 vertices was attached with labels during the training and they
491 were used to calculate the loss and gradients. The vertices with

492 ³ <https://pytorch-geometric.readthedocs.io/en/1.5.0/index.html>

Table 4

Dataset overview. \bar{d} represents the average vertex degree. $\text{dim}(\mathbf{v})$ is the dimension of the input feature vector.

Dataset	$ \mathcal{V} $	$ \mathcal{E} $	\bar{d}	$\text{dim}(\mathbf{v})$	#Class	Directed
pubmed (pub) [28]	19,717	44,324	4.5	500	3	Yes
amazon-photo (amp) [33]	7,650	119,081	31.1	745	8	Yes
amazon-computers (amc) [33]	13,752	245,861	35.8	767	10	Yes
coauthor-physics (cph) [33]	34,493	247,962	14.4	8415	5	Yes
flickr (fli) [31]	89,250	899,756	10.1	500	7	No
com-amazon (cam) [34]	334,863	925,872	2.8	32	10	No

unseen labels were used in the evaluation and inference phase to evaluate the accuracy of GNN models.

Datasets. We used six real-world graph datasets as listed in Table 4 that were popular in the GNN accuracy evaluation [28,31,33,34]. For directed graphs, PyG converted them into undirected ones during data loading. Thus, the average degree of a directed graph $\bar{d} = \frac{2|\mathcal{E}|}{|\mathcal{V}|}$. For an undirected graph, the average degree was defined as $\bar{d} = \frac{|\mathcal{E}|}{|\mathcal{V}|}$. For the cam dataset, its vertices were not associated with feature vectors. Thus, we generated random dense feature vectors for it and excluded it from accuracy evaluation. For amp, amc, cph, and cam, we used 70%/15%/15% of the samples as the training/evaluation/test set, respectively. For pub, we used 500/1000 vertices as the evaluation/test set and the remained as the training set according to [28]. For fli, we used 50%/25%/25% of the samples as the training/evaluation/test set according to [31]. We also used random graphs generated by the R-MAT graph generator [35] in some experiments, to explore the effects of graph topological characteristics (like average degrees) on performance bottlenecks. Input feature vectors of random graphs were random dense vectors with a dimension of 32. Vertices of random graphs were classified into 10 classes randomly.

GNN Implementation. We implemented the four typical GNNs: GCN, GGNN, GAT, and GaAN. To compare performance characteristics of the four GNNs side-by-side, we used a unified GNN structure for them: Input Layer → GNN Layer 0 → GNN Layer 1 → Softmax Layer (to prediction). The structure was popular in the experimental evaluation of GCN [1], GAT [6], and GaAN [7]. Since a GGNN layer required the input and output hidden vectors had the same dimension, we added two multi-layer perceptron (MLP) layers to transform the dimensions of the input/output feature vectors: Input Layer → MLP → GGNN Layer 0 → GGNN Layer 1 → MLP → Softmax Layer. Unless otherwise specified, we stored the dataset and the model parameters on the GPU side. The GNN training was conducted also on the GPU side.

Hyper-parameters. We used $\text{dim}(\mathbf{x})$ to denote the dimension of a vector \mathbf{x} . We picked the hyper-parameters of GNNs according to their popularity in their references [1,4,6,7]. Unless otherwise mentioned, we used the same set of hyper-parameters for all the datasets. Some hyper-parameters (like dimensions of hidden vectors) were common in the four GNNs and we set them to the same values. For GCN/GAT/GaAN, we set $\mathbf{h}_x^0 = \mathbf{v}_x$, $\text{dim}(\mathbf{h}_x^1) = 64$, and $\text{dim}(\mathbf{h}_x^2) = \#\text{Class}$ (the number of classes in the dataset). For GAT, the first GAT layer contained 8 heads, and the attention vector of each head had a dimension of 8. The first GAT layer merged attention vectors of 8 heads by concatenating. The second GAT layer used a single head with a dimension of $\#\text{Class}$. For GGNN, we set $\text{dim}(\mathbf{h}_x^0) = \text{dim}(\mathbf{h}_x^1) = \text{dim}(\mathbf{h}_x^2) = 64$. We used 8 heads in the both GaAN layers with $d_a = d_v = 8$, and $d_m = 64$.

We used Adam [36] as the gradient descent optimizer with a learning rate of 0.01 and a weight decay of 1e-5. We initialized weights in GNNs using the method described in [37] and initialized bias as zeros. Without otherwise mentioned, in the experiments related to accuracy evaluation, we trained all GNNs for a maximum of 100 k epochs and used the early stopping criterion according to

[33]: the training was stopped if the validation loss did not improve for 50 epochs. We chose the model parameters that achieved the lowest validation loss as the final model parameters. The accuracy of the test set was evaluated with the final model.

Sampling Techniques. We picked the neighbor sampler from GraphSAGE [5] and the cluster sampler from ClusterGCN [26] as the typical sampling techniques. For the neighbor sampler, we set the neighborhood sample sizes of the GNN layer 0 and the GNN layer 1 to 10 and 25, respectively. We set the default batch size to 512, according to [5]. For the cluster sampler, we partitioned the input graph into 1500 partitions and used 20 partitions per batch, according to [26].

3.2. Experimental scheme

To find out performance bottlenecks in GNN training, we conducted the experimental analysis with four questions. The answers to those questions would give us a more comprehensive view of the performance characteristics of GNN training.

Q1 *How did the hyper-parameters affect the training/inference time, memory usage and accuracy of a GNN?* (Section 4.1)
Every GNN had a group of hyper-parameters, such as the number of GNN layers and the dimensions of hidden feature vectors. The hyper-parameters affected the processing time per epoch and peak memory usage during training and inference. They also affected the accuracy of a GNN. Larger hyper-parameter values usually meant more model parameters and more complex models. To evaluate their effects, we measured how the training/inference time per epoch, the peak memory usage (of the GPU), and the test accuracy changed as we increased the values of the hyper-parameters. Through the experiments, we verified the validity of the time complexity analysis in Table 2 and Table 3. The complexity analysis allowed us to analyze performance bottlenecks theoretically.

Q2 *Which stage was the most time-consuming stage in GNN training and inference?* (Section 4.2)
We decomposed the GNN training/inference time on different levels: the layer level, the edge/vertex calculation level, and the basic operator level. On each level, we decomposed the time of an epoch into several stages. The most time-consuming stage was the performance bottleneck. Optimizing its implementation would significantly reduce the training time.

Q3 *Which consumed most of memory in GNN training and inference?* (Section 4.3)
The limited memory capacity of a GPU prevented us from conducting training/inference on big graphs. We measured the peak memory usage during GNN training/inference under different graph scales, input feature dimensions, and average degrees. Based on the results, we analyzed which was the most memory-consuming component in a GNN. Reducing its memory usage would enable us to train GNNs on bigger graphs under the same memory capacity.

598
 599 Q4 Could sampling techniques remove performance bottlenecks in
 600 GNN training/inference? Did the use of sampling techniques in
 601 training sacrifice model accuracy? (Section 4.4)
 602 Theoretically, sampling techniques could significantly
 603 reduce the number of graph neurons that participated in
 604 the training of a batch. Consequently, the processing time
 605 and memory usage per batch should also decrease. The
 606 model accuracy of GNNs might also be affected. To validate
 607 the effectiveness of sampling techniques, we measured the
 608 training/inference time, peak memory usage, and test accu-
 609 racy under different batch sizes. If sampling techniques were
 610 effective, they would be the keys to conduct GNN training/
 611 inference on very big graphs. If they were not effective, we
 612 wanted to find out which impaired their efficiency.
 613

4. Evaluation results and analysis

614 We answer the four questions in Section 3.2 one by one with
 615 experiments. Without otherwise mentioned, the reported training
 616 time per epoch was the average wall-clock training time of 50
 617 epochs, excluding abnormal epochs. During the training of some
 618 epochs, there were extra profiling overheads from NVIDIA Nsight
 619 Systems and GC pauses from the Python interpreter that signifi-
 620 cantly increased the training time. We denoted the 25% and 75%
 621 quantiles of the training time of 50 epochs as Q1 and Q3, respec-
 622 tively. We regarded the epochs with the training time outside the
 623 range of $[Q1 - 1.5 * (Q3 - Q1), Q3 + 1.5 * (Q3 - Q1)]$ as abnor-
 624 mal epochs.
 625

4.1. Effects of hyper-parameters on performance

626 The hyper-parameters of a GNN (such as the dimensions of hid-
 627 den vectors and the number of heads) determined the model com-
 628 plexity of the GNN. They affected the training/inference time,
 629 memory usage, and accuracy of the GNN at the same time.
 630

4.1.1. Effects on training time

631 According to Tables 2 and 3, the time complexity of the messag-
 632 ing function ϕ and the updating function γ was linear to each
 633 hyper-parameter separately. If we increased one of the hyper-
 634 parameters and fixed the others, the training time should increase
 635 linearly in theory.
 636

To verify the time complexity analysis in Tables 2 and 3, we first compared the training time of the four GNNs in Fig. 5. The ranking of the training time was GaAN \gg GAT ($>$ GGNN $>$ GCN in all cases). Since the real-world graphs had more edges than vertices ($|\mathcal{E}| > |\mathcal{V}|$), the time complexity of the edge calculation stage affected more obviously than the vertex calculation stage. The ranking was consistent with the time complexity analysis.
 643

To further evaluate effects of hyper-parameters on training time, we measured the training time of each GNN with varying hyper-parameters in Figs. 6–9.
 644

645 For GCN and GGNN, $\dim(\mathbf{h}_x^0)$ and $\dim(\mathbf{h}_x^1)$ were solely deter-
 646 mined by the dataset with $d_{in}^0 = \dim(\mathbf{h}_x^0) = \dim(\mathbf{v}_x)$ and
 647 $d_{out}^1 = \dim(\mathbf{h}_x^2) = \#\text{Class}$. Therefore, the only modifiable hyper-
 648 parameter was the dimension of \mathbf{h}_x^1 that affected the dimension of output hidden vectors of the layer 0 d_{out}^0 and the dimension of input hidden vectors of the layer 1 d_{in}^1 simultaneously, i.e.
 649 $\dim(\mathbf{h}_x^1) = d_{out}^0 = d_{in}^1$. According to the time complexity analysis, if we fixed other hyper-parameters but only increased $\dim(\mathbf{h}_x^1)$, the computational costs of the GNN layer 0 and the GNN layer 1 should both increase linearly with $\dim(\mathbf{h}_x^1)$, causing the training time of the whole GNN also increased linearly. Figs. 6 and 7 show that the training time of GCN and GGNN increased linearly with
 650

$\dim(\mathbf{h}_x^1)$ when $\dim(\mathbf{h}_x^1)$ was big, consistent with the theoretical analysis.
 651

For GAT, we modified the number of heads K and the dimension of each head d_{head} in the GAT layer 0. The dimension of \mathbf{h}_x^1 was determined as $\dim(\mathbf{h}_x^1) = Kd_{head}$. Thus, the computational costs of the GAT layer 0 and the GAT layer 1 should increase linearly with K and d_{head} separately. Fig. 8 confirms the theoretical analysis.
 652

For GaAN, it was also based on the multi-head mechanism. Its time complexity should be affected by $\dim(\mathbf{h}_x^1)$ ($d_{out}^0 = d_{in}^1 = \dim(\mathbf{h}_x^1)$), d_a , d_v , d_m , and the number of heads K . Fig. 9 demonstrates that the training time increased linearly with the hyper-parameters, except for $\dim(\mathbf{h}_x^1)$. As $\dim(\mathbf{h}_x^1)$ increased, the training time increased first slightly and then linearly. We observed similar phenomena in GCN, GGNN, and GAT: When the values of hyper-parameters were too low, GNN training could not make full use of the computing power of the GPU. When the values of hyper-parameters became high enough, training time increased linearly, supporting the time complexity analysis.
 653

4.1.2. Effects on inference time

654 For all GNNs, we found that the effects of hyper-parameters on
 655 the inference time were the same as the training time. Taking
 656 GGNN as an example, Fig. 10 shows the effects of hyper-
 657 parameters on the inference time of GGNN. By cross-comparing
 658 Fig. 10 and Fig. 7, the trends of the inference time and training time
 659 were the same: as $\dim(\mathbf{h}_x^1)$ increased, the vertex and edge calcula-
 660 tion time both grew linearly when $\dim(\mathbf{h}_x^1)$ was large enough. For
 661 the other GNNs, we observed similar phenomena. The results indi-
 662 cated that the complexity analysis presented in Tables 2 and 3
 663 were also applicable to inference.
 664

4.1.3. Effects on peak memory usage

665 We further measured the effects of hyper-parameters on the
 666 peak GPU memory usage during training in Fig. 11. The memory
 667 usage also increased linearly as the hyper-parameters increased
 668 for all GNNs, except for GaAN on $\dim(\mathbf{h}_x^1)$. As the hidden vectors
 669 \mathbf{h}_x^1 in GaAN consumed a small proportion of memory, the growth
 670 in the memory usage was not noticeable until $\dim(\mathbf{h}_x^1)$ was large
 671 enough. The effects of hyper-parameters on the inference memory
 672 usage were the same as the training. Taking GAT as an example,
 673 Fig. 12 shows that the peak memory usage during inference grew
 674 linearly with the increasing hyper-parameters. By cross-
 675 comparing Figs. 12 and 11c, the hyper-parameters affected the
 676 peak memory usage of training and inference in the same way.
 677 For the other GNNs, we observed similar phenomena.
 678

4.1.4. Effects on accuracy

679 The values of hyper-parameters determined the model com-
 680 plexity of a GNN. The relationships between model complexity
 681 and accuracy were complex. Generally speaking, higher model
 682 complexity brought more powerful representation capability and
 683 might bring higher accuracy, but it also increased the risk of
 684 overfitting.
 685

686 To evaluate the effects of hyper-parameters on accuracy, we
 687 measured the accuracy of the typical GNNs with varying hyper-
 688 parameters in Fig. 13. For GCN, its accuracy was sensitive to the
 689 dimension of hidden vectors $\dim(\mathbf{h}_x^1)$. As $\dim(\mathbf{h}_x^1)$ increased, the
 690 accuracy first increased quickly and then stabilized when
 691 $\dim(\mathbf{h}_x^1) \geq 8$. For GGNN, its accuracy curves showed similar trends
 692 as GCN, but GGNN was more sensitive to $\dim(\mathbf{h}_x^1)$ than GCN. Its
 693 accuracy even decreased when $\dim(\mathbf{h}_x^1) \geq 1024$. Since the model
 694 complexity of GGNN was high (with 13 weight matrices/vectors
 695



Fig. 5. Distribution of the wall-clock training time of 50 epochs on different datasets. GaAN crashed due to the out of memory exception on the cph dataset.

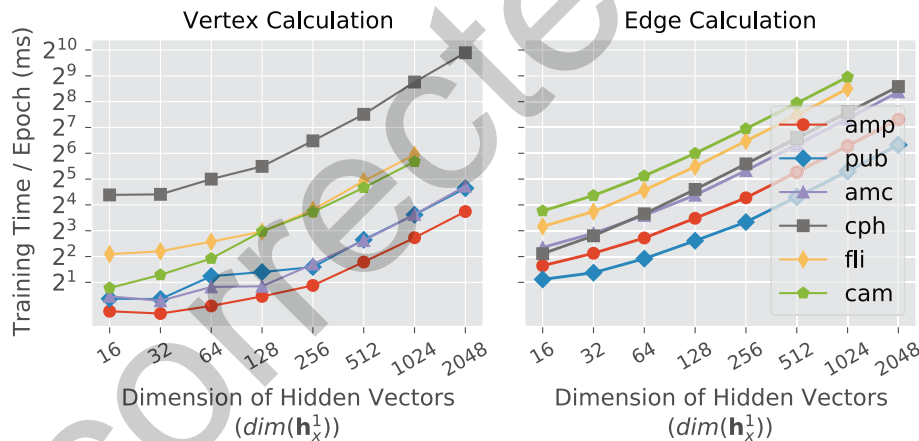


Fig. 6. Effects of hyper-parameters on the vertex/edge calculation time of GCN in training.

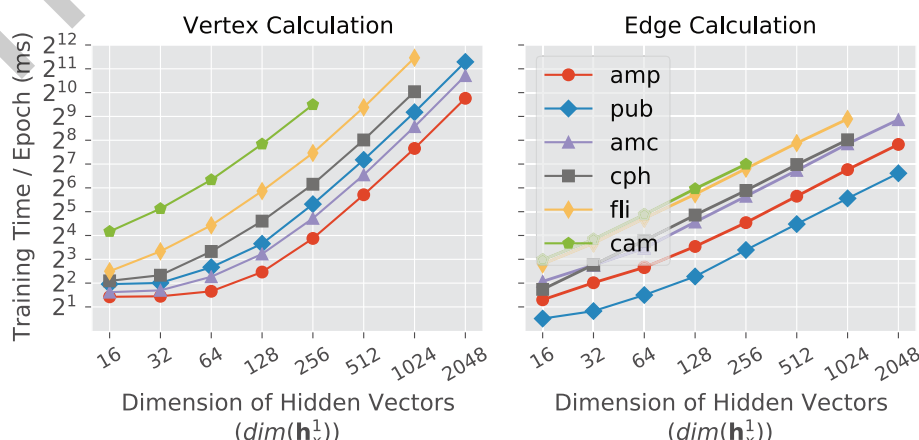
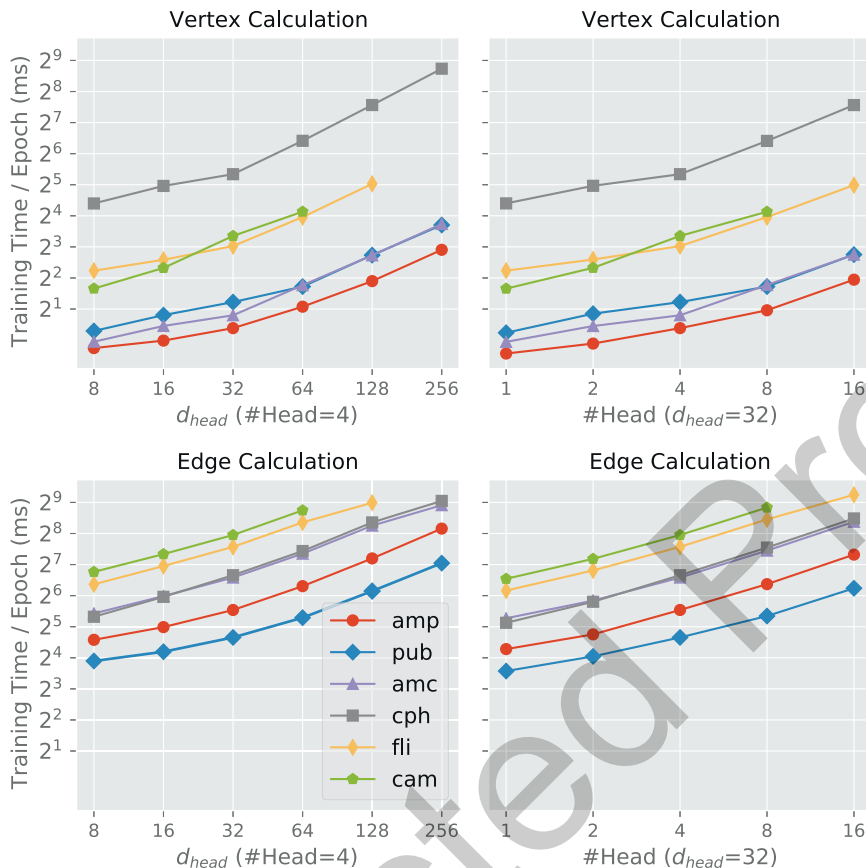
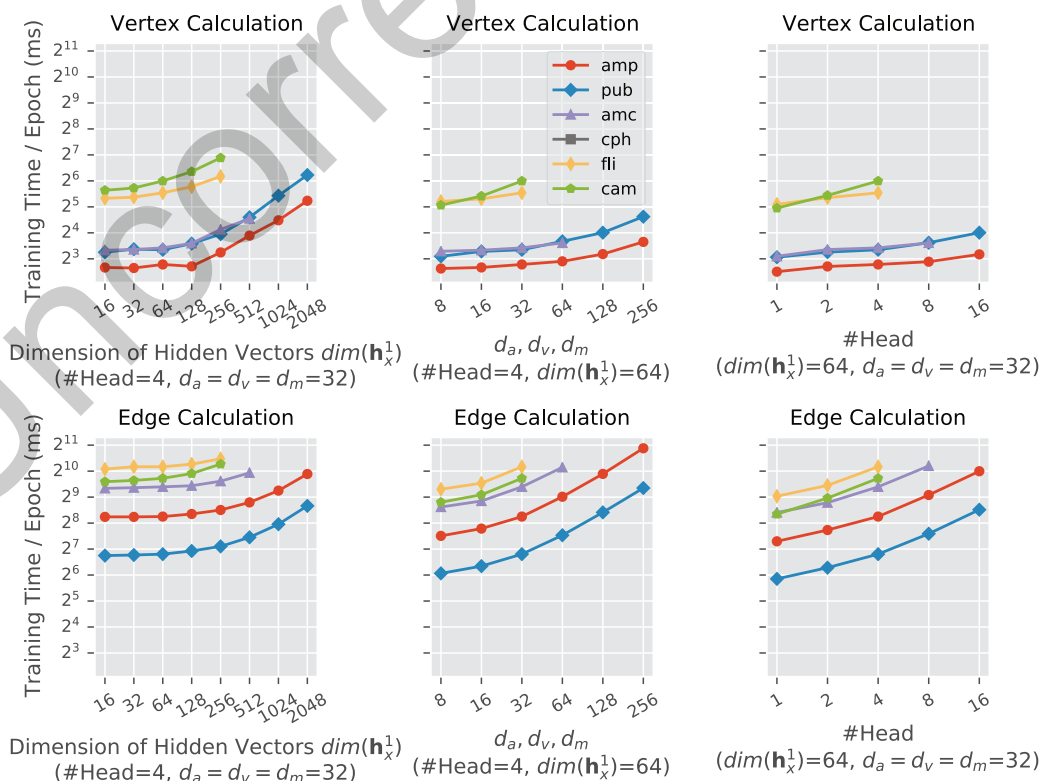


Fig. 7. Effects of hyper-parameters on the vertex/edge calculation time of GGNN in training.

**Fig. 8.** Effects of hyper-parameters on the vertex/edge calculation time of GAT in training.**Fig. 9.** Effects of hyper-parameters on the vertex/edge calculation time of GaAN in training.

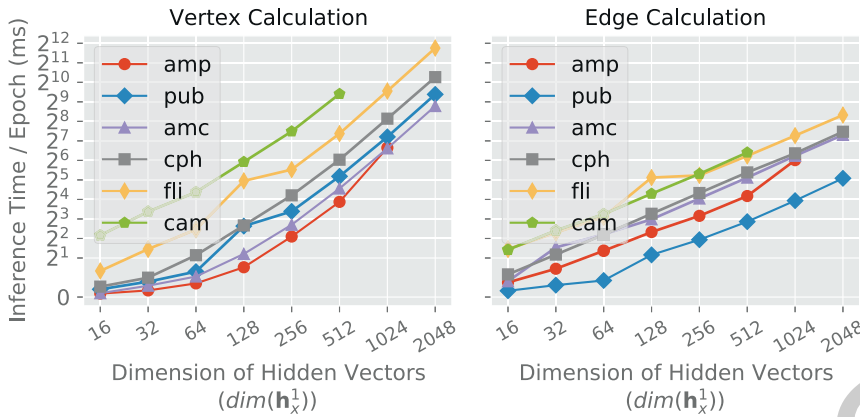


Fig. 10. Effects of hyper-parameters on the vertex/edge calculation time of GGNN in inference.

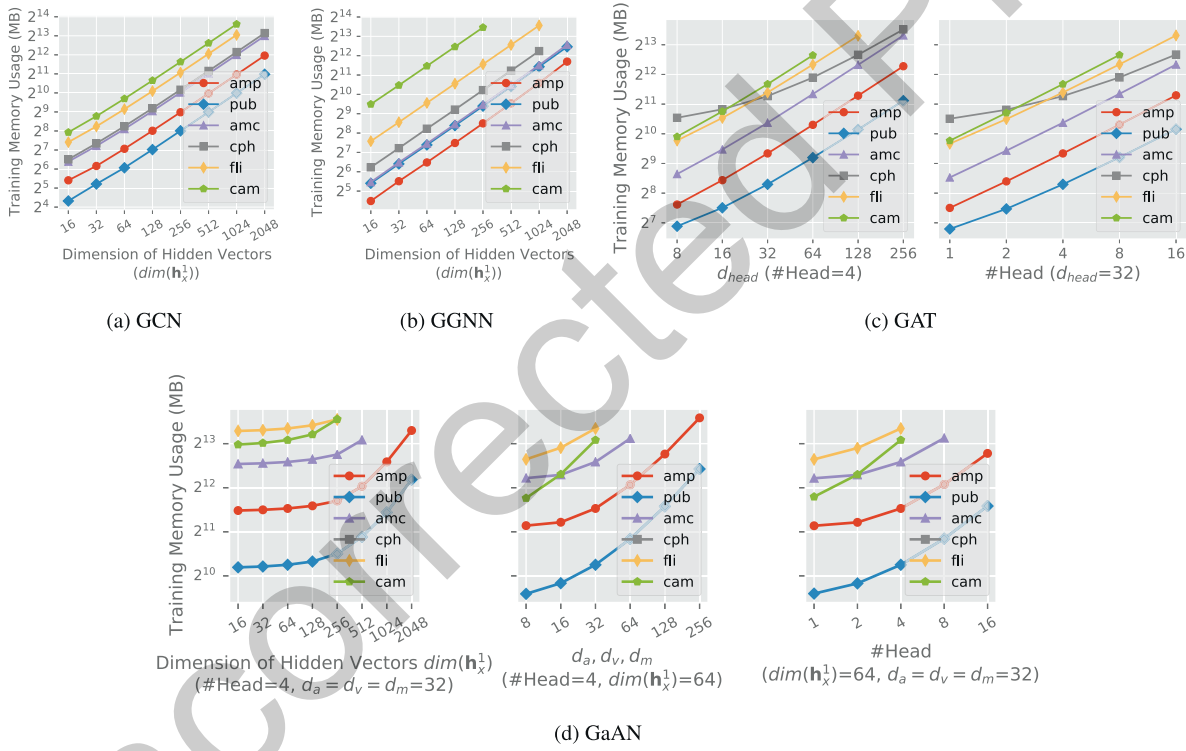


Fig. 11. Effects of hyper-parameters on the peak GPU memory usage during training, excluding the memory used by the dataset and the model parameters.

to train), GGNN might occur overfitting in those cases. For GAT, its accuracy was more sensitive to the dimension of each head d_{head} than the number of heads. For GaAN, only $\text{dim}(\mathbf{h}_x^1)$ showed obvious impacts on accuracy. The experimental results indicated that the accuracy of the GNNs was often low when $\text{dim}(\mathbf{h}_x^1)$ (for GCN/GGNN/GaAN) or d_{head} (for GAT) was very low. As $\text{dim}(\mathbf{h}_x^1)$ or d_{head} increased to a certain threshold, the GNNs gained sufficient learning ability to achieve stable accuracy.

Fig. 14 further compares the best accuracy that every GNN achieved on different datasets. The best accuracy of the four GNNs was very close. It was also close to the accuracy reported in [33,31]. The results indicated that there was no clear winner. The relative accuracy between GNNs varied greatly with different datasets. GaAN achieved the highest accuracy in three out of five datasets.

GCN achieved the highest or second-highest accuracy in three out of five datasets, though its model was simplest. Simple GNN models (such as GCN) could still achieve good accuracy with proper hyper-parameter settings.

Summary. The complexity analysis in Tables 2 and 3 was valid for both training and inference. Fixing other hyper-parameters, each hyper-parameter itself affected the training/inference time and the memory usage of a GNN layer in a linear way. Algorithm engineers could adjust hyper-parameters according to the complexity analysis to avoid explosive growth in the training/inference time and memory usage. The accuracy of GNNs was much more sensitive to the dimension of hidden vectors/heads than the other hyper-parameters. The relative accuracy between GNNs varied greatly with different datasets. Simple GNN models (such as GCN) could achieve good accuracy with proper hyper-parameter settings.

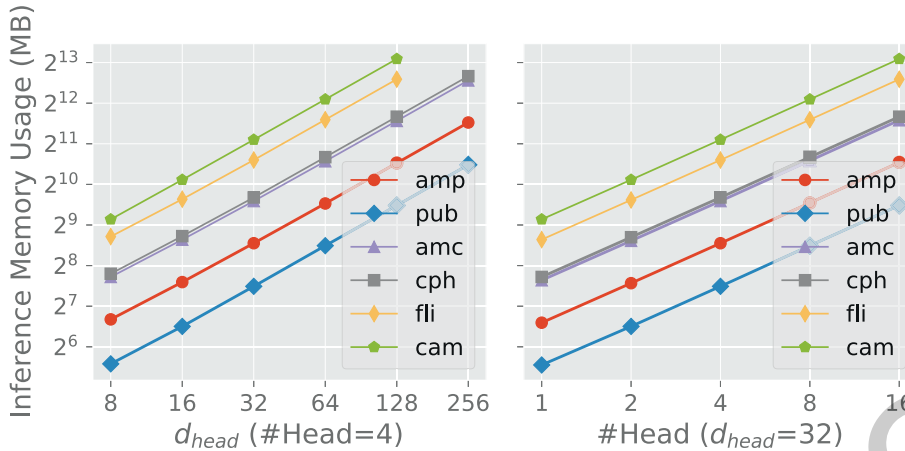
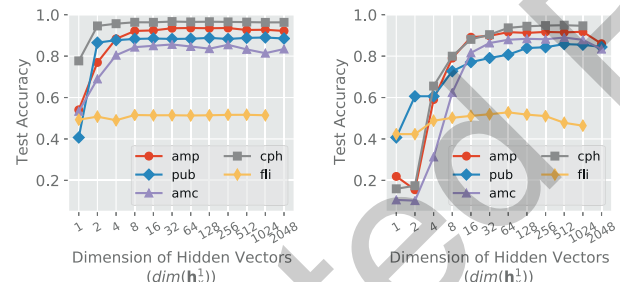
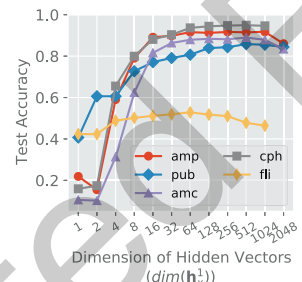


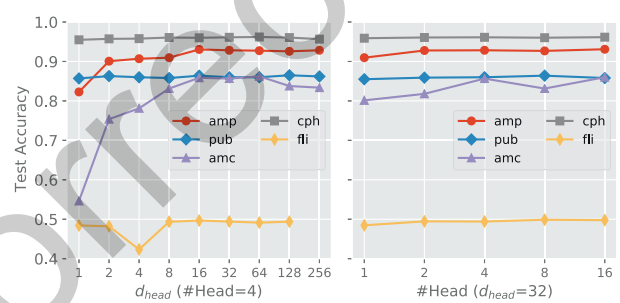
Fig. 12. Effects of hyper-parameters on the peak GPU memory usage during inference of GAT, excluding the memory used by the dataset and the model parameters.



(a) GCN



(b) GGNN



(c) GAT

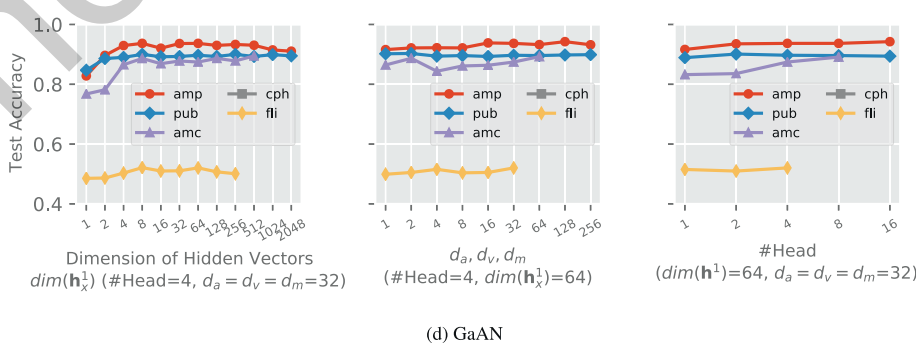


Fig. 13. Effects of hyper-parameters on the accuracy of the typical GNNs.

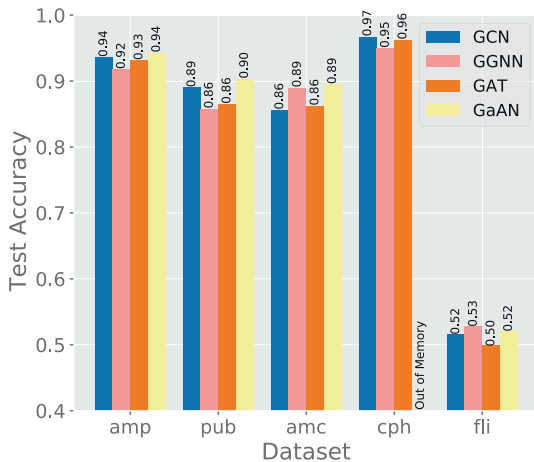


Fig. 14. Best accuracy that each GNN achieved on different datasets.

746

4.2. Time breakdown analysis

747

To find out which stage/step dominated the training/inference time, we decomposed the training/inference time and analyzed performance bottlenecks level by level. We first analyzed the training time in Sections 4.2.1–4.2.3. The similarities and differences between training and inference were analyzed in Section 4.2.4.

752

4.2.1. Layer level

753

Fig. 15 decomposes the training time of a GNN on the layer level. The training time of each layer was the summation of the time in the forward, backward, and evaluation phases. In GCN, GAT, and GaAN, the time spent on the layer 0 was much larger than

754

755

756

the layer 1. In those GNNs, the dimensions of the input/output hidden vectors in the layer 0 were much larger than the dimensions in the layer 1: $d_{in}^0 = \dim(\mathbf{v}_x)$, $d_{out}^0 = d_{in}^1 = 64$, $d_{out}^1 = \#Class$, and $\dim(\mathbf{v}_x) \gg \#Class$. For GaAN, since it required the dimensions of the input/output hidden vectors must be the same, the hyper-parameters were set to $d_{in}^0 = d_{out}^0 = d_{in}^1 = d_{out}^1 = 64$ and the training time of both layers was close.

Each GNN layer was further divided into the vertex and edge calculation stages. In **Fig. 15**, GCN spent most of the training time on the edge calculation stage on most datasets. A special case was the cph dataset. The dimension of the input feature vectors was very high in cph, making the vertex calculation stage of the GCN Layer 0 spend considerable time. GGNN also spent the majority of its training time on the edge calculation stage, but the high time complexity of its vertex updating function γ^l made the proportion of the vertex calculation in the total training time much higher than the other GNNs. For GAT and GaAN, due to their high edge calculation complexity, the edge calculation stage was the dominant stage.

The experimental results also indicated that the average degree of the dataset affected the proportion of the edge/vertex calculation time in the total training time. For GaAN, the time spent on the vertex calculation stage exceeded the edge calculation stage on the pub and cam datasets, because the average degrees of the two datasets were low, making $|\mathcal{E}|$ and $|\mathcal{V}|$ much closer. To evaluate the effects of the average degree, we generated random graphs with 50,000 vertices and average degrees ranging from 2 to 100. **Fig. 16** shows the training time of the four GNNs under different average degrees. As the average degree increased, the training time of the edge calculation stage grew linearly. For GCN, GAT, and GaAN, the edge calculation stage dominated the entire training time even when the average degrees were small. Only for GGNN that had high vertex and low edge calculation complexity, the

757
758
759
760
761
762
763
764
765
766
767
768
769
770
771
772
773
774
775
776
777
778
779
780
781
782
783
784
785
786
787
788
789

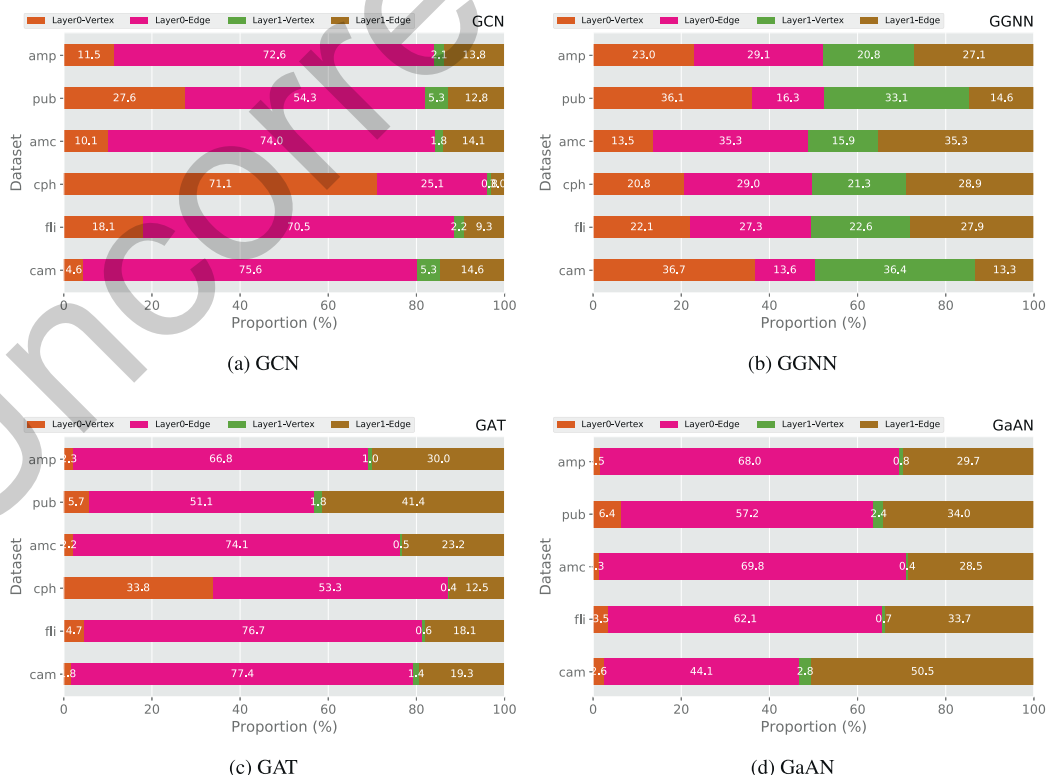


Fig. 15. Training time breakdown on the layer level. The training time of each layer included the time spent on the forward, backward, and evaluation phases. Each layer was further decomposed into the vertex and edge calculation stages.

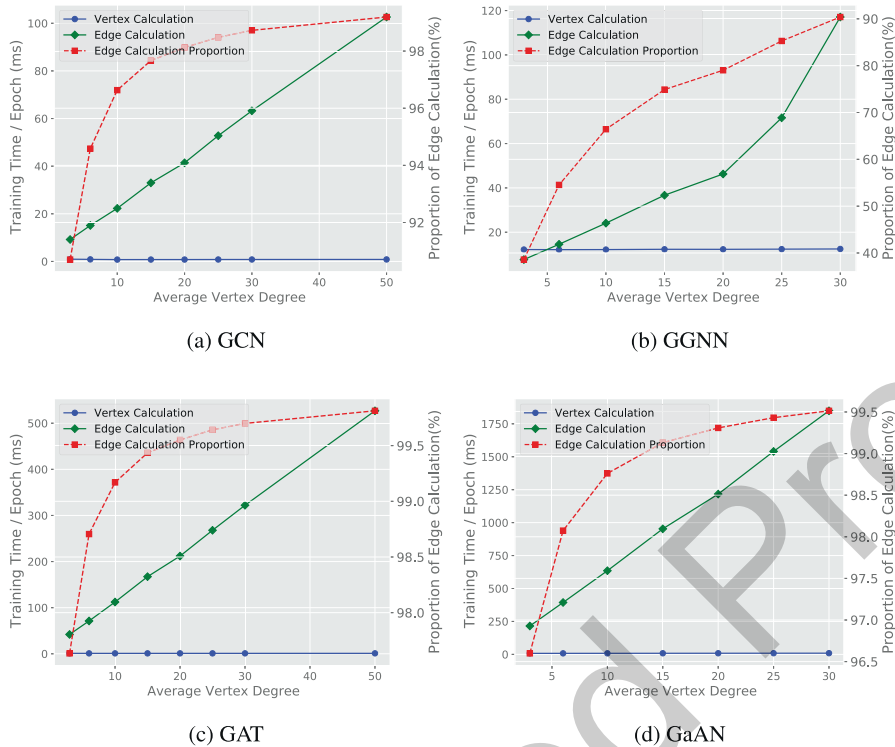


Fig. 16. Effects of average degrees on the vertex/edge calculation time. Graphs were generated with the R-MAT generator by fixing the number of vertices as 50,000.

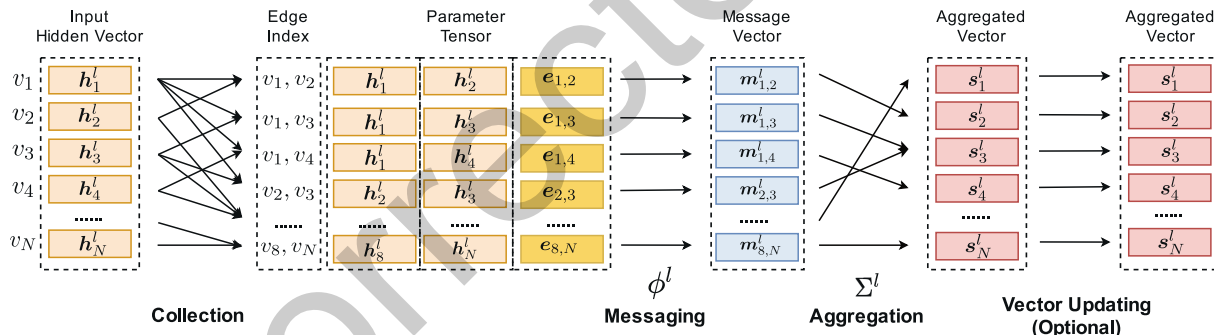


Fig. 17. Step decomposition of the edge calculation stage of the GNN layer l .

790 training time of the vertex calculation stage exceeded the edge calculation stage under low average degrees (<5).
791

792 In summary, the edge calculation stage was the most time-
793 consuming stage in GNN training. Improving its efficiency was the
794 key to reduce the GNN training time.

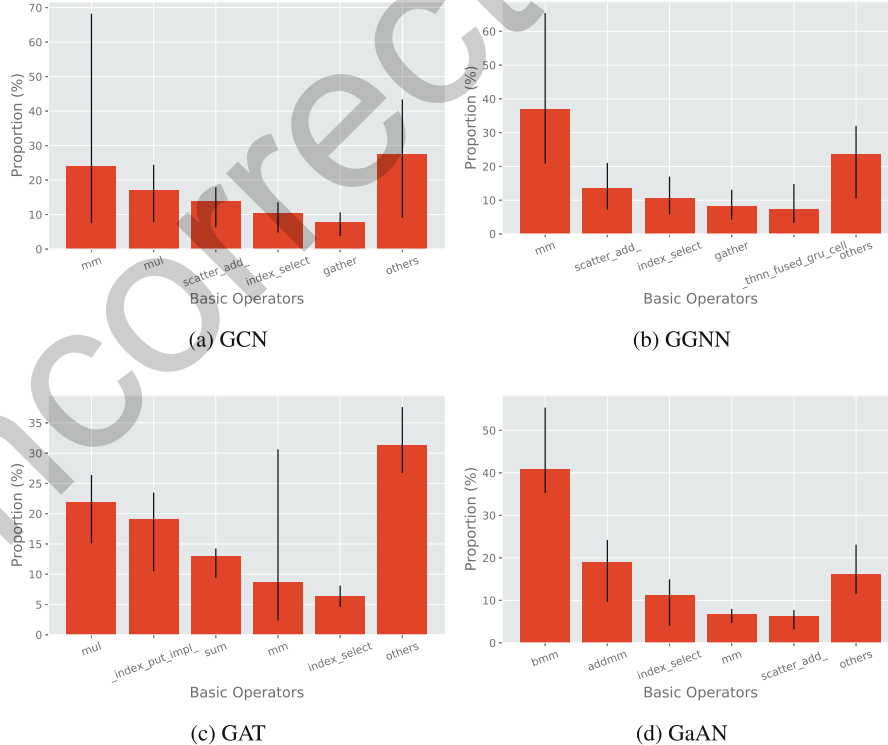
795 4.2.2. Step level in edge calculation

796 We further investigated the most time-consuming step of the
797 edge calculation stage. In the implementation of PyG, the edge cal-
798 culation stage consisted of four steps: collection, messaging, aggre-
799 gation, and vector updating, as shown in Fig. 17. The edge index
800 was a matrix with $|\mathcal{E}|$ rows and two columns. It held the edge set
801 of the graph. The two columns of the edge index stored the source
802 and the target vertex IDs of each edge. The collection step copied
803 the hidden vectors from the previous GNN layer h_y^l and h_x^l to the
804 both endpoints of each edge $e_{y,x}$ in the edge index, forming the
805 parameter tensor $[h_y^l, h_x^l, e_{y,x}]$ of the messaging function ϕ^l . This step
806 only involved data movement. The messaging step called the mes-

807 saging function ϕ^l on all edges to get message vectors $m_{y,x}^l$. The
808 aggregation step aggregated the message vectors with the same
809 target vertex into an aggregated vector s_y^l . The vector updating step
810 was optional. It performed an additional transformation on the
811 aggregated vectors (for example, adding the bias in GCN).

812 We decomposed the execution time of the edge calculation
813 stage in Fig. 18. In each GNN, the proportions of the four steps were
814 rather stable, rarely affected by datasets. For GAT and GaAN with
815 the high edge calculation complexity, the messaging step con-
816 sumed most of the training time. For GCN and GGNN with the
817 low edge complexity, the proportions of the steps were close. Since
818 the messaging function ϕ^l of GGNN used the pre-computed \hat{h}_y^l as
819 the message vector directly, the time spent on the messaging step
820 of GGNN was negligible. Although the collecting step did not con-
821 duct any computation and only involved data movement, it occu-
822 pied a noticeable execution time in the four GNNs.

823 The results indicate that the performance bottlenecks of the edge
824 calculation stage depend on the complexity of the messaging function
825 ϕ . When the time complexity of ϕ was high, the messaging step

**Fig. 18.** Training time breakdown of the edge calculation stage.**Fig. 19.** Top 5 time-consuming basic operators in training. The time proportion of each basic operator was averaged over all datasets with the error bar indicating the maximum and the minimum.

826
827
828
829

was the performance bottleneck. Optimizing the implementation of ϕ could significantly reduce training time. Otherwise, the collection and the aggregation steps were performance bottlenecks. Improving the efficiency of the two steps could benefit all GNNs.

4.2.3. Operator level

The functions ϕ, Σ and γ in the edge and vertex calculation stages were made up of a series of basic operators implemented on the GPU side, such as the matrix multiplication mm , the elemen-

831
832
833

twise multiplication `mul` and the index-based selection `index_select`. Fig. 19 shows the top-5 time-consuming basic operators of training each GNN, averaged over all datasets.

GCN. The most time-consuming basic operator was the matrix multiplication `mm` used in the vertex updating function γ . The elementwise multiplication `mul` used in the messaging function ϕ was also time-consuming. The other three operators were used in the edge calculation stage: `scatter_add_` for the aggregation step in the forward phase, `gather` for the aggregation step in the backward phase, and `index_select` for the collection step. For GCN, the basic operators related to the edge calculation stage consumed the majority of the training time.

GGNN. The top basic operator was `mm` used in the vertex updating function γ . Due to its high time complexity, the proportion of `mm` was much higher than the other operators. The `thnn_fused_gru_cell` operator was used in both the forward and backward phases of γ . The other three operators were used in the edge calculation stage.

GAT. All the top basic operators except for `mm` were related to the edge calculation stage. The `mm` operator was used in the vertex updating function γ .

GaN. The top basic operator was `bmm` used in the messaging function ϕ . The `addmm` operator and the `mm` operator were used in both the vertex and the edge calculation stages, where the edge calculation stage was dominant.

The most time-consuming operators in the four GNNs were the matrix multiplication `mm` and the elementwise multiplication `mul`, making GNN training suitable for GPUs. Although the aggregation step in the edge calculation stage was relatively simple (like sum and mean), the related operators—`scatter_add` and `gather`—still consumed a certain amount of the time. The two operators had to synchronize between hardware threads to avoid updating the same aggregated vector at the same time. They also conducted non-regular memory access with the access pattern determined by the edge set dynamically. For GPUs, they were less efficient than `mm`. The index-based selection operator `index_select` used in the collection step consumed about 10% of the training time in all GNNs. Improving the efficiency of `scatter_add/gather/index_select` could benefit all kinds of GNNs.

4.2.4. Comparing inference and training

We found that the performance characteristics of GNN inference were highly similar to training on the *layer* level and the *step* level. Taking GCN as an example, Fig. 20 shows the time breakdowns of GCN inference on the *layer* level and *step* level of the edge calculation. By cross-comparing Fig. 15a with Fig. 20a, Fig. 16a with Fig. 20b, and Fig. 18a with Fig. 20c, the time breakdowns of training and inference were very similar. For the other GNNs, we observed similar phenomena.

The main differences between training and inference were reflected in two aspects: the wall-clock time and the top time-consuming basic operators. The inference time was much less than the training time. Fig. 21 compares the wall-clock time of training and inference on the `amp`, `amc`, and `fli` datasets. The results on the other datasets were similar. Since the inference only conducted the forward propagation from the input layer to the prediction layer, the inference time was very close to the time of the forward phase in training. The inference time was 34% (GCN), 32% (GGNN), 25% (GAT), and 32% (GaN) of the training time, averaged over all datasets.

The top time-consuming basic operators of training and inference also showed a certain degree of difference. Some of the top time-consuming operators during training were replaced by new operators in inference. Fig. 22 shows the top 5 time-consuming basic operators in inference. For GCN, the `index` operator used in the prediction layer became the new top 5 time-consuming oper-

ators, replacing the `gather` operator used in the backward phase in training. For GGNN, `index` operator in the prediction layer also became a time-consuming basic operator. For GAT, the `input_put_impl` operator (used in the backward phase) in Fig. 19c was replaced by the `scatter_add` operator used in the forward edge calculation in Fig. 22c. For GaAN, the `mm` operator was replaced by the `cat` operator used in the vertex updating function.

Although some specific time-consuming operators were different, the performance bottlenecks on the operator level were the same for training and inference. The matrix multiplication `mm` and the element-wise multiplication `mul` operators were still time-consuming for inference, making GNN inference also suitable for GPUs. The basic operators related to the collection and aggregation steps in the edge calculation still consumed non-trivial time in inference.

Summary of Time Breakdown Analysis. The GNN training/inference was suitable for GPUs. The edge calculation stage was the main performance bottleneck in most cases, except for processing GNNs with high vertex calculation complexity on low-average-degree graphs. The performance bottlenecks in the edge calculation stage depended on the time complexity of the messaging function ϕ . If the time complexity of ϕ was high, ϕ dominated the training/inference time of the edge calculation stage. Optimizations should focus on improving its efficiency. Otherwise, the collection step and the aggregation step dominated the training/inference time. The collection step suffered from lots of data movement. The aggregation step suffered from data synchronization and non-regular data access.

4.3. Memory usage analysis

Training. During the GNN training, we stored all data (including datasets and intermediate results) in the on-chip memory of the GPU. Compared with the main memory on the host side (90 GB), the capacity of the GPU memory (16 GB) was very limited. *The GPU memory capacity limited the scales of the graphs that it could handle.* For example, GaAN was unable to train on the `cph` dataset due to the out of memory exception.

Fig. 23 shows the peak memory usage of each phase during the GNN training on the `amp` dataset. The trends on the other datasets were similar. *The GNN training achieved its peak memory usage in the forward and the backward phases.* The forward phase generated lots of intermediate results. Some key intermediate results were cached for the gradient calculation in the backward phase, increasing memory usage. For example, Fig. 24 shows the computation graph of the vertex updating function γ^l of GGNN. Each operator in the computation graph generated an intermediate tensor. Some key intermediate tensors were cached. The cached tensors were the main source of memory usage in the loss phase. By the end of the backward phase, the cached tensors were released. Since the evaluation phase did not have to calculate the gradients, it did not cache intermediate tensors. Its memory usage declined sharply.

The peak memory usage during the GNN training far exceeded the size of the dataset itself. We defined the *memory expansion ratio* (MER) as the ratio of the peak memory usage during the training to the memory usage after loading the dataset. Fig. 25 compares MER of different GNNs. GCN had the lowest MER (up to 15.2) while GaAN had the highest MER (up to 104.6). *The high MERs limited the data scalability of GNNs*, making GPUs unable to handle big graphs. Fig. 25 also indicates that the same GNN had different MERs for different datasets. Two characteristics of a dataset affected the MER: the dimension of the input feature vectors and the average degree of the graph.

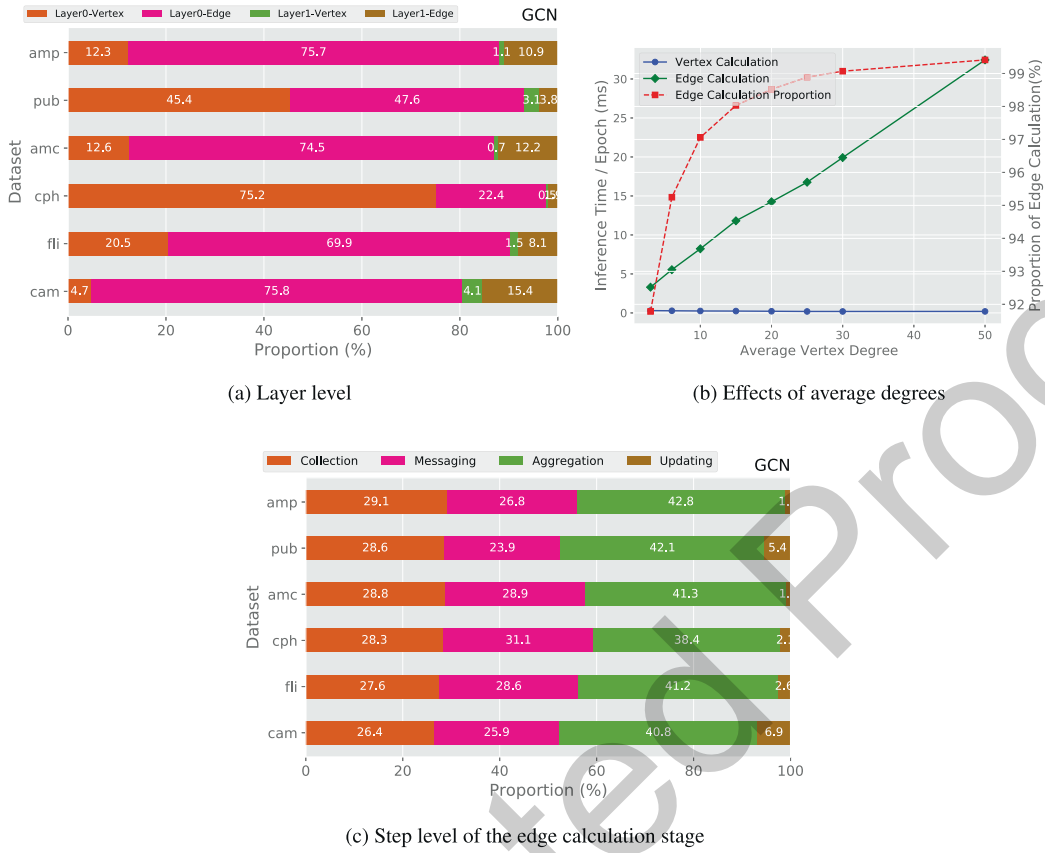


Fig. 20. Time breakdowns of GCN inference.

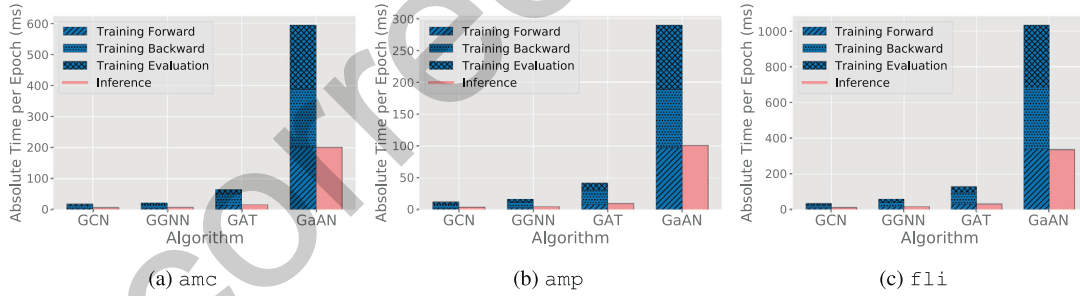


Fig. 21. Wall-clock inference time on different datasets.

To find out how the dimension of input feature vectors affected the MER, we generated random input feature vectors with different dimensions for the `cam` dataset and measured the MER in Fig. 26. Under the same hyper-parameters, the MER decreased as the dimension of input feature vectors increased. When the dimension of the input feature vectors was high, the size of the dataset itself was large. The size became comparable to the size of intermediate results, making MERs low.

Average degrees also affected MERs by influencing the relative sizes of intermediate results from the edge and the vertex calculation stages. Fixing the number of vertices $|\mathcal{V}|$, we generated random graphs with different average degrees. Fig. 27 shows how the memory usage changed according to the average degree. As the average degree \bar{d} increased, the peak memory usage increased linearly with \bar{d} . The edge calculation stage gradually dominated the memory usage and the MER converged to a stable value. The stable value was determined by the complexity of the edge calculation

stage. Except for GGNN, the MERs of the other GNNs increased as \bar{d} increased. As GGNN had high vertex calculation complexity, the MERs related to the vertex calculation stage were much higher than the edge calculation stage. When the edge calculation stage dominated the memory usage, its MERs became smaller.

We also fixed the number of edges $|\mathcal{E}|$ and generated random graphs with different $|\mathcal{V}|$. Fig. 28 shows how the memory usage changed according to $|\mathcal{V}|$. MERs of all GNNs were insensitive to $|\mathcal{V}|$, compared to $|\mathcal{E}|$. Except for GGNN, the MERs of the other GNNs declined as $|\mathcal{V}|$ increased because the sizes of the datasets increased more quickly than the sizes of the intermediate results. As GGNN had high vertex calculation complexity, the sizes of the intermediate results were very sensitive to $|\mathcal{V}|$. It indicated that the intermediate results of the edge calculation stage dominated the memory usage during the GNN training.

Inference. Fig. 29 shows the memory expansion ratios of typical GNNs during inference. Since no intermediate results had to be

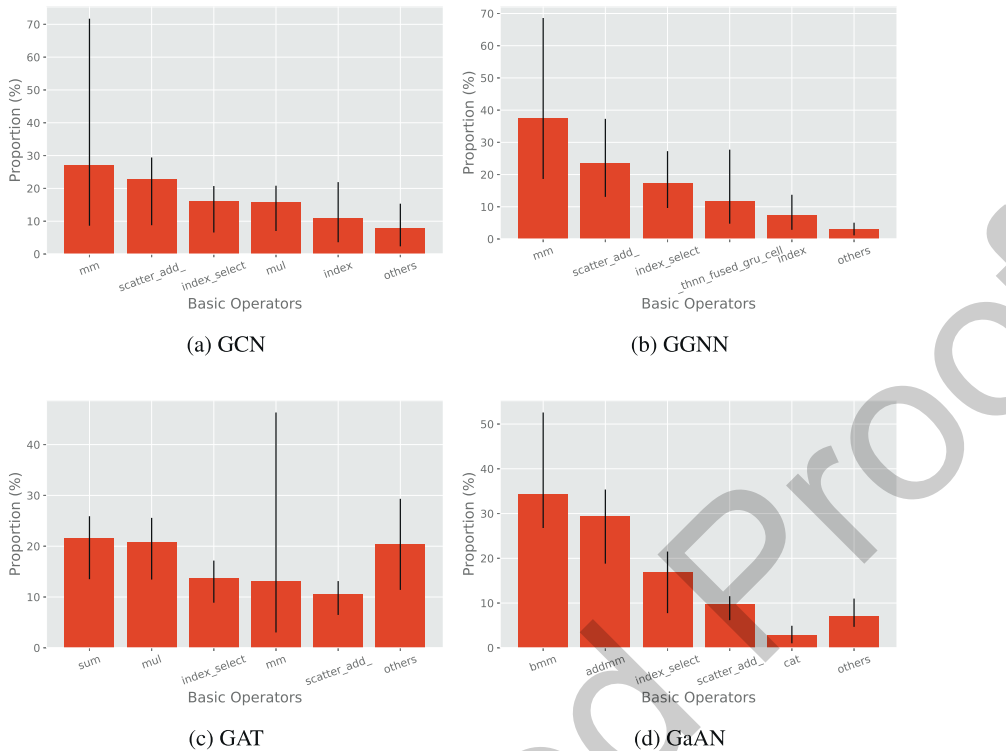


Fig. 22. Top 5 time-consuming basic operators in inference. The time proportion of each basic operator was averaged over all datasets with the error bar indicating the maximum and the minimum.

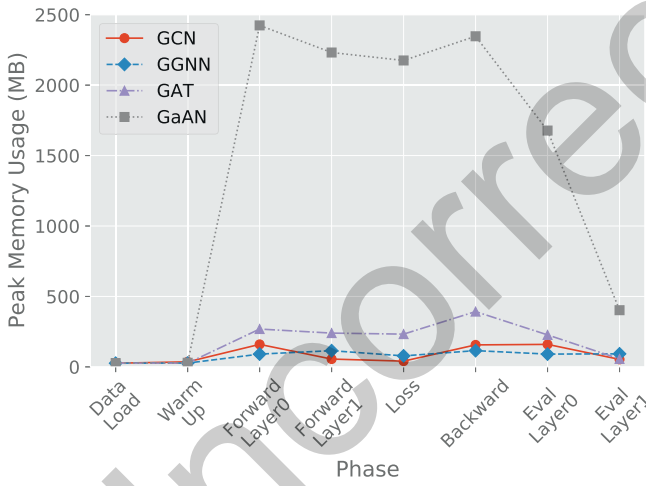


Fig. 23. Memory usage of each phase during the GNN training. Dataset: amp.

cached during inference of GGNN, GAT, and GaAN, the MERs of inference were much less than training for the three GNNs (compared with Fig. 25). The MERs of inference were 45–83% (GGNN), 52–61% (GAT), and 37–69% (GaAN) of training. However, the MERs were still high, disallowing inferencing with big graphs. To handle big graphs, the sample-based inference was necessary.

We also conducted experiments about the effects of input feature dimensions, average degrees, and the number of vertices on the memory usage of inference. The results were similar to GNN training.

Summary of Memory Usage Analysis. The high memory expansion ratio severely restricted the data scalability of GNN training and inference. The memory usage mainly came from the intermediate results of the edge calculation stage. Fixing the number of vertices,

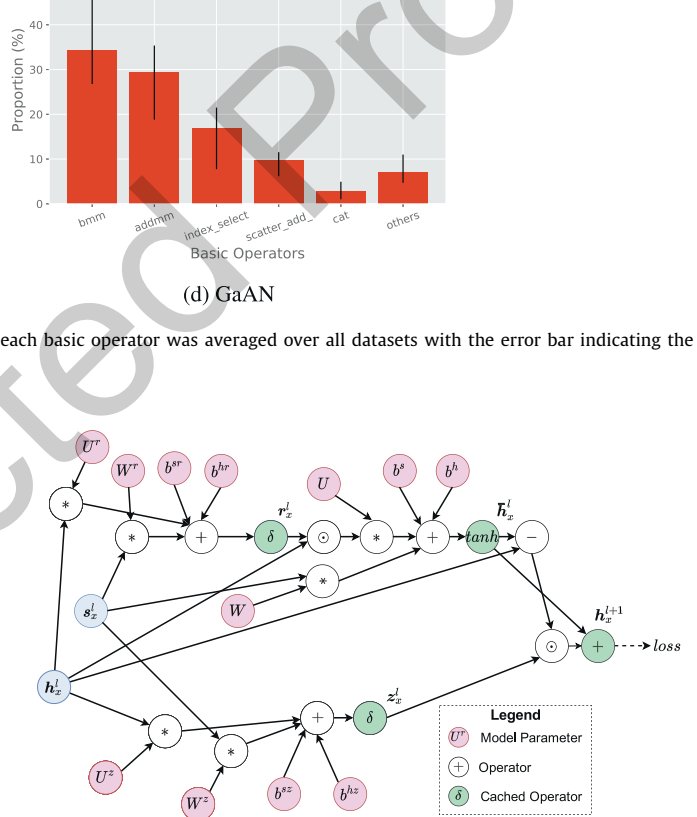


Fig. 24. Computation graph of the vertex updating function γ of GGNN.

the memory usage increased linearly along with the number of edges. Fixing the GNN structure and the hyper-parameters, increasing the dimension of input feature vectors could reduce the memory expansion ratio. To reduce the memory usage of GNN training and inference, optimizations should focus on reducing memory footprints of the edge calculation stage.

4.4. Effects of sampling techniques on performance

With the sampling techniques, GNNs were trained and performed inference in a mini-batch manner. Each epoch was decomposed into many batches. In each batch, PyG only sent the sampled subgraph to the GPU to train or inference. The batch size determined the size of the sampled subgraph. Thus, it affected the accuracy, training/inference time, and memory usage simultaneously.

1009
1010
1011
1012
1013
1014

1015
1016
1017
1018
1019
1020
1021

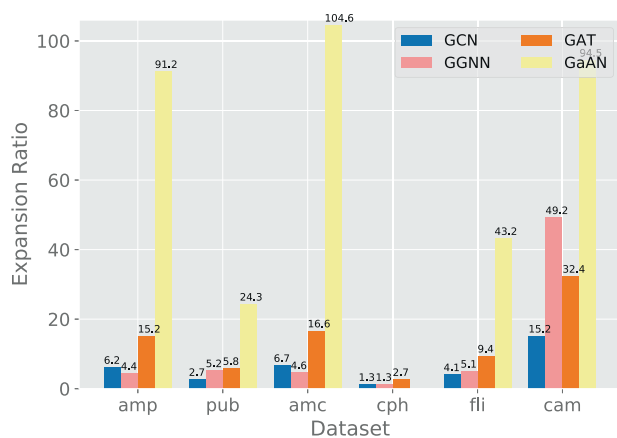


Fig. 25. Memory expansion ratios of typical GNNs.

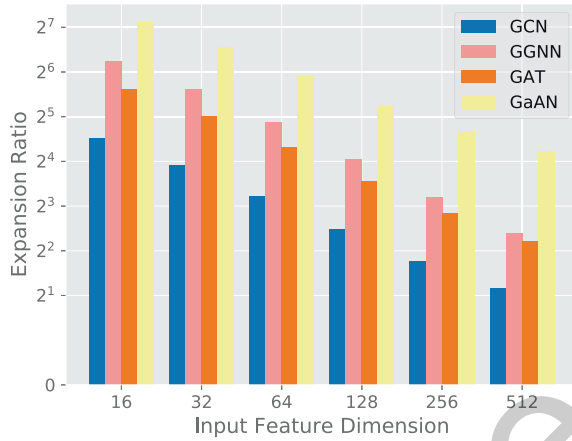


Fig. 26. Memory expansion ratio under different dimensions of input feature vectors. Dataset: cam.

4.4.1. Size of sampled subgraphs

Fig. 30 shows how the size of the sampled subgraph changed with the batch size. For the neighbor sampler, the relative batch size was defined as the proportion of the sampled vertices of the last GNN layer in \mathcal{V} . For the cluster sampler, the relative batch size was defined as the proportion of the sampled partitions in all

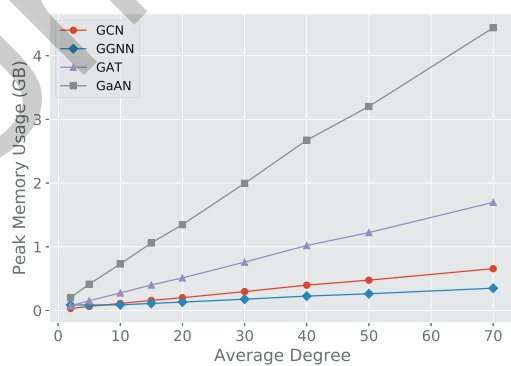
partitions of the graph. The experimental results indicated that the neighbor sampler was very sensitive to the batch size. As the batch size increased, the size of the sampled subgraph first increased quickly and then stabilized. The cluster sampler was much less sensitive compared to the neighbor sampler. The number of vertices and the average degree of the sampled subgraphs increased linearly with the batch size.

The average degree of the sampled subgraph was much lower than the average degree of the original graph, especially when the relative batch size was low. Taking the neighbor sampler with the relative batch size of 6% as an example, the average degree of the amp dataset was 31.1, but the average degree of the sampled subgraph was only 5.8. For the cluster sampler, the average degree was 3.0. Fig. 31 compares the degree distribution of the sampled subgraphs with the original graph. The slopes of the curves were similar, indicating that the sampled subgraphs still followed the power-law degree distribution. However, the numbers of high-degree vertices were much less than the original graph, lowering the average degrees. According to the experimental results in Section 4.2, if the average degree became lower, the proportion of the training time spent on the vertex calculation stage would become higher, especially for GGNN.

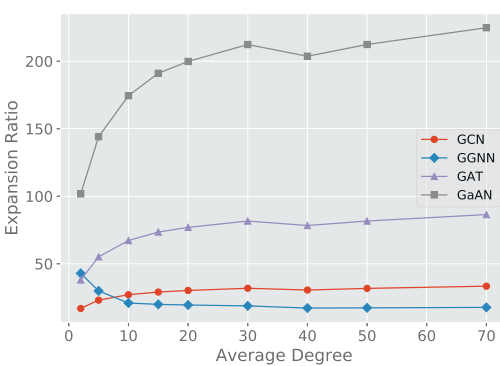
4.4.2. Performance bottlenecks in sample-based training

To find out performance bottlenecks of the sampling techniques, we decomposed the training/inference time per batch into three phases: *sampling* on the CPU side, *transferring* sampled subgraphs from the CPU side to the GPU side, and *training/inference* with the sampled subgraphs on the GPU side.

Fig. 32 shows the *training* time breakdown of the four GNNs under different relative batch sizes. For the neighbor sampler, the sampling technique reduced the training time per batch only when the batch size was very small. When the batch became bigger, the sampling and the data transferring phases introduced noticeable overheads, making the training time exceed the full-batch training. For the clustering sampler, the sampled subgraph was smaller than the neighbor sampler under the same relative batch size. The reduction in the training time was more obvious than the neighbor sampler. However, the overheads increased quickly as the relative batch size increased. The training time under the 25% relative batch size already exceeded the time of full-batch training. The experimental results indicated that the current implementation of the sampling techniques in PyG was inefficient. When the batch size was large, more than 50% of the time had been spent on sampling and data transferring. *The sampling techniques were only efficient under small batch sizes.*

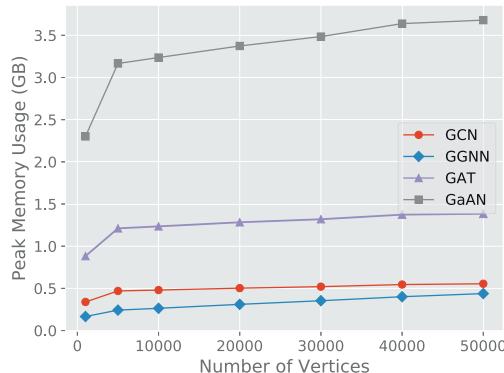


(a) Peak memory usage

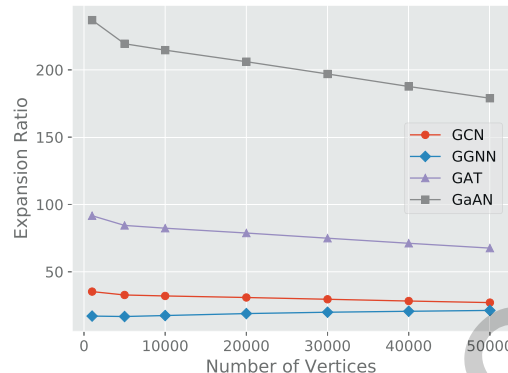


(b) Memory expansion ratio

Fig. 27. Memory usage under different average degrees. The random graphs were generated by fixing the number of vertices at 10 K and the dimension of input feature vectors at 32.



(a) Peak memory usage



(b) Memory expansion ratio

Fig. 28. Memory usage under different numbers of vertices. The random graphs were generated by fixing the number of edges at 500 K and the dimension of input feature vectors at 32.

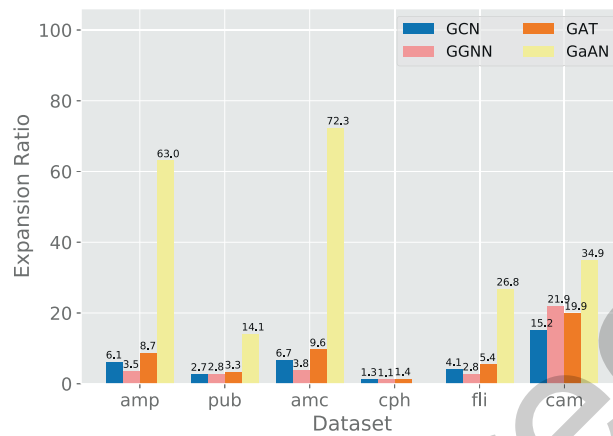


Fig. 29. Memory expansion ratios of typical GNNs in inference.

The main advantage of the sampling techniques was reducing the peak memory usage during training. Fig. 33 shows the memory usage under different batch sizes. The peak memory usage declined significantly even under big batch sizes. The sampling techniques made training GNNs on big graphs possible for GPUs.

The disadvantage of the sampling technique was wasting GPU resources. As the sampling techniques were only effective under small batch sizes, the sampled subgraphs were very small in those cases. They could not make full use of the computing power of a GPU. To simulate the situation, we generated random graphs with few vertices and measured their training time per epoch in Fig. 34. As the number of vertices increased, the training time was almost unchanged except for GaAN. The training time of GaAN increased only when $|V| \geq 4000$.

4.4.3. Performance bottlenecks in inference

The sample-based inference was an effective technique to conduct inference on big graphs. Taking the node classification task as an example, to predict labels for a given set of vertices $V_{predict}$, the inference sampler sampled a subgraph containing complete L -hop neighborhoods of all vertices in $V_{predict}$, where L was the number of GNN layers. Since the real-world graphs often had small-world property, the size of the sampled subgraph increased quickly as the number of vertices in $V_{predict}$ (i.e., batch size) increased. Fig. 35 shows how the relative batch size ($\frac{|V_{predict}|}{|V|}$) affected the aver-

age degree and the number of edges of the sampled subgraphs during inference. When the relative batch size was 10%, the number of edges in the sampled subgraphs were close to the number of edges in the whole graph in most datasets. To limit the memory usage during inference, the batch size used should be very small in inference.

However, the overheads brought by sampling and data transferring from CPU to GPU became obvious when the batch size was small. Fig. 36 shows the time breakdowns of sample-based inference on different datasets. On the amp and cam datasets, the sampling time even accounted for near half of the total inference time. The results indicated that the current implementation of inference sampler in PyG was also inefficient. Improving its efficiency could significantly reduce the sample-based inference time.

4.4.4. Effects on accuracy

Since the size of the sampled subgraph was much smaller than the original graph, the accuracy of the GNN models trained with sampling techniques might be different from the full-batch training. To find out how the batch size affected the test accuracy, we trained GNNs with different batch sizes. Figs. 37 and 38 compare the test accuracy achieved by sampling techniques with the test accuracy of the full-batch training. For each combination of dataset and GNN, we chose the hyper-parameters that achieved the highest accuracy according to the experimental results in Section 4.1.4.

The experimental results confirmed the effectiveness of the sampling methods in terms of accuracy. When the relative batch size was greater than or equal to 3%, the test accuracy of the GNNs trained with sampling was close to the accuracy obtained by full-batch training. In most cases, the accuracy achieved by the sampling techniques was slightly lower than the full-batch training. However, there were some exceptions (like GaAN in Figs. 38a and 38b) that the accuracy achieved by sampling was even higher.

The relationships between batch size and test accuracy were complex. A larger batch size did not always bring higher accuracy. For example, the accuracy of GaAN in Fig. 38a and GGNN in Fig. 38c decreased as the batch size increased. A smaller batch size sometimes could achieve higher accuracy. For example, GAT achieved a higher accuracy with 1% relative batch size than the full-batch training in Fig. 38b. Given a sampling method, we found that the optimal batch size highly depended on the dataset and the GNN algorithm. Our observations were similar to [31]. How to automatically select a proper batch size is a topic worth further studying.

Among the two sampling methods, the performance of the cluster sampler was more stable than the neighbor sampler. With the

1098
1099
1100
1101
1102
1103
1104
1105
1106
1107
1108
1109
1110
1111
1112
1113
1114
1115
1116
1117
1118
1119
1120
1121
1122
1123
1124
1125
1126
1127
1128
1129
1130
1131
1132
1133
1134
1135
1136
1137
1138
1139
1140

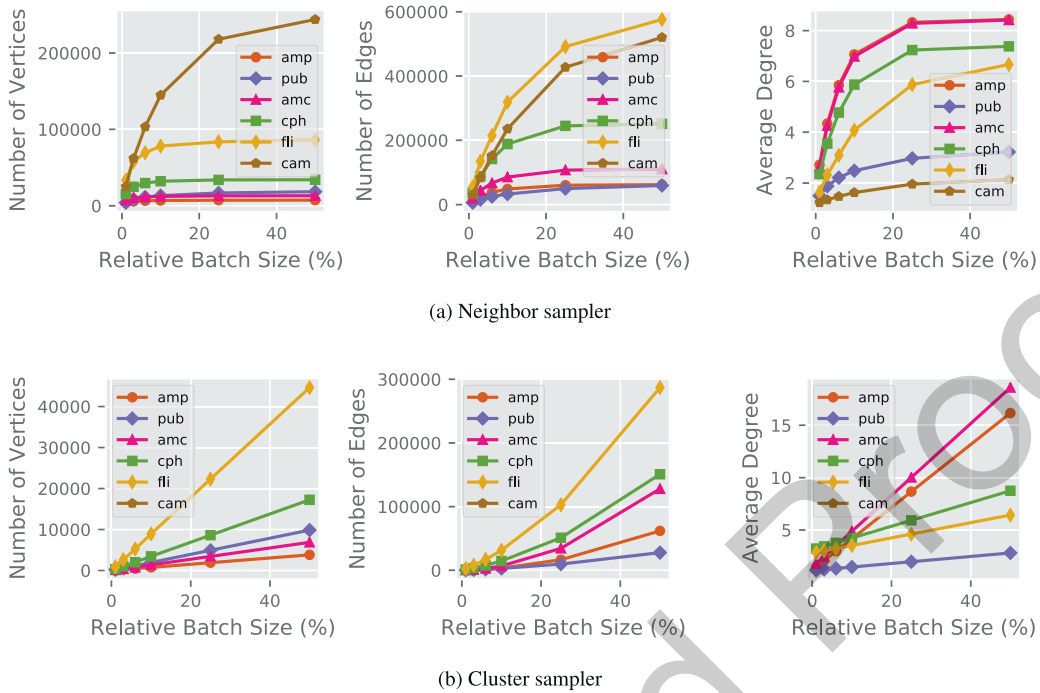


Fig. 30. Sizes of sampled subgraphs under different relative batch sizes. The batch size was relative to the full graph. Each batch size was sampled 50 times and the average values were reported. The error bar indicates the standard deviation.

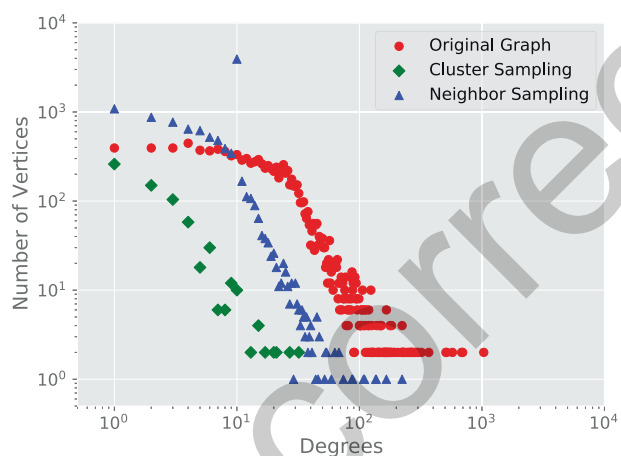


Fig. 31. Vertex degree distribution of the sampled subgraph (relative batch size: 6%) and the original graph. Dataset: amp.

cluster sampler, the test accuracy of different GNNs was very close to the accuracy of full-batch training. With the neighbor sampler, the test accuracy of different GNNs showed more obvious differences.

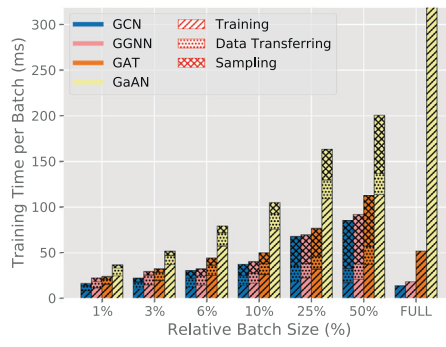
Summary of Sampling Techniques. The sampled subgraphs produced by the neighbor sampler and the cluster sampler had lower average degrees than the original graph. With small batch sizes, the sampling techniques could significantly reduce the peak memory usage per batch. However, the current implementation of the sampling techniques in PyG was inefficient to handle small batches. The time spent on the sampling phase and the data transferring phase could even exceed the training/inference phase. Small batches could not make full use of the computing power of a GPU either.

5. Insights

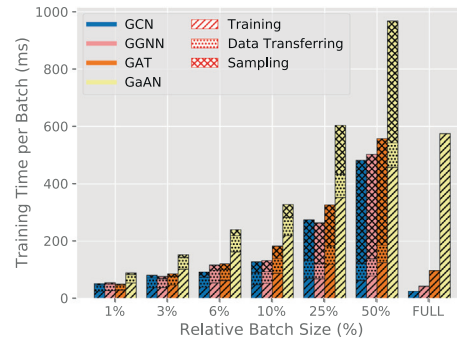
Through the extensive experiments, we propose the following key findings and suggestions for how to optimize the performance for GNN training and inference.

1. *The time complexity in Tables 2 and 3 points out performance bottlenecks theoretically.* The experimental results validate the time complexity analysis. The time complexity points out where the bottleneck comes from. Optimization should focus on complex operations in the messaging function ϕ and the vertex updating function γ .
2. *The computational cost of a GNN layer is mainly affected by the dimensions of the input and output hidden vectors.* Theoretically and empirically, the training and inference time and the memory usage of a GNN layer both increase linearly with the dimensions of the input/output hidden vectors separately. GNNs are friendly to high-dimensional scenarios. Algorithm engineers can use high-dimensional feature vectors to improve the expressive power of a GNN without worrying about exponential growth in the training/inference time and memory usage.
3. *Performance optimizations should focus on improving the efficiency of the edge calculation stage.* The edge calculation stage is the most time-consuming stage in most GNNs.
 - If the complexity of the messaging function ϕ is high, the implementation of ϕ is critical to performance. Improving its efficiency can significantly reduce training/inference time. For example, the attention mechanism in GNNs (like GAT and GaAN) requires an extra sub-layer to calculate the attention weight of each edge. Implementing the attention mechanism with specially optimized basic operators on the GPU side is a potential optimization direction.
 - If the complexity of ϕ is low, the efficiency of the collection step and the aggregation step becomes critical. The existing GNN libraries [15,14,16] already introduce the fused operator to improve their efficiency. When the messaging function

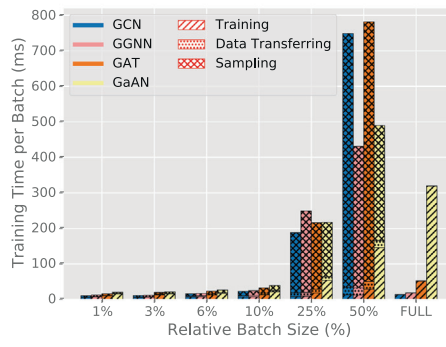
1155
1156
1157
1158
1159
1160
1161
1162
1163
1164
1165
1166
1167
1168
1169
1170
1171
1172
1173
1174
1175
1176
1177
1178
1179
1180
1181
1182
1183
1184
1185
1186
1187
1188



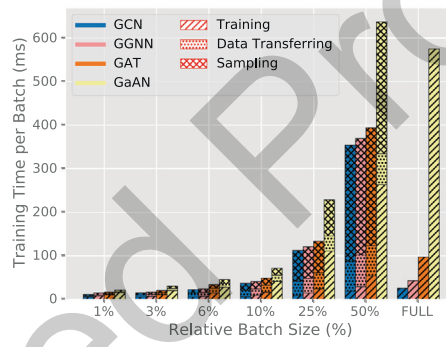
(a) Neighbor sampler on amc



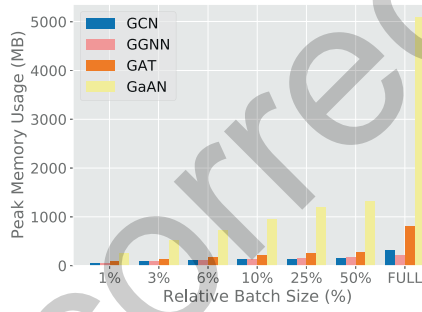
(b) Neighbor sampler on fli



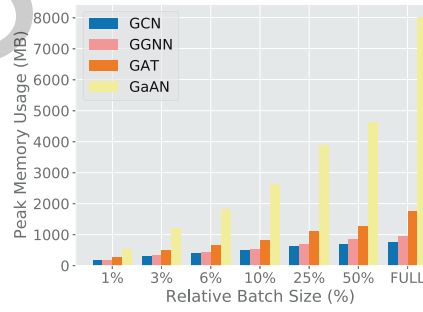
(c) Cluster sampler on amc



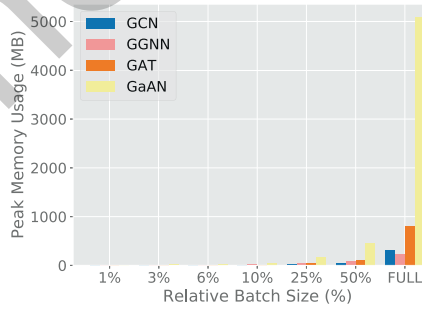
(d) Cluster sampler on fli

Fig. 32. Training time per batch breakdown. FULL means that the full graph participates in the training.

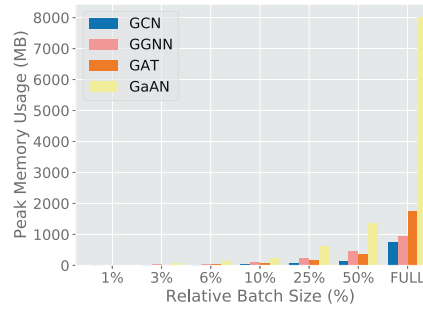
(a) Neighbor sampler on amc



(b) Neighbor sampler on fli



(c) Cluster sampler on amc



(d) Cluster sampler on fli

Fig. 33. Peak memory usage under different batch sizes. FULL means that the full graph participated in the training.

ϕ is an assignment or a scalar multiplication of the input hidden vector of the source vertex, the libraries replace the collection, messaging, and aggregation steps with a single

fused operator. The fused operator calculates the aggregated vectors directly from the input hidden vectors, minimizing the memory footprints and overlapping the memory access-

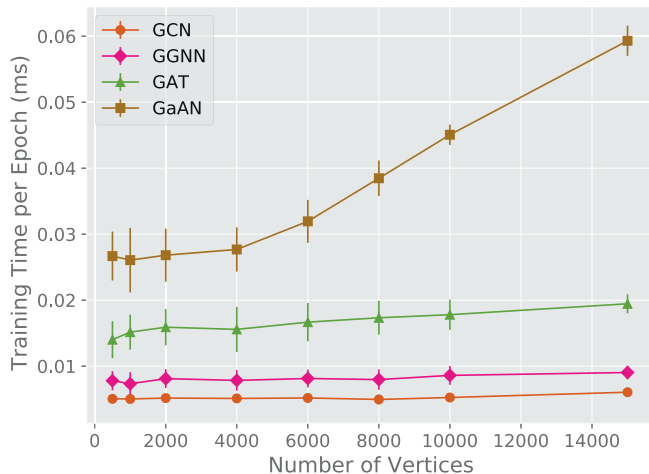


Fig. 34. Training time per epoch on small random graphs. For each number of vertices, we generated 50 random graphs with an average degree of 4.0 and reported the average training time per batch (without the evaluation phase). The error bar indicates the standard deviation.

ing with computation. In this way, it significantly reduces the training/inference time of GNNs with low edge calculation complexity (like GCN) [19,20]. However, the applicable condition of the fused operator is very restricted. It does not work for ϕ with more complex operations like matrix multiplication. A potential optimization is to develop composite CUDA kernels that can read the input hidden vectors and aggregate message vectors on the fly, without materializing the parameter vectors and the message vectors.

4. *The high memory usage caused by the intermediate results of the edge calculation stage limits the data scalability of GNN training/inference.* The memory expansion ratios of the typical GNNs are very high, making GPUs unable to handle big graphs. One solution is to distribute the dataset among several GPUs and frequently swap parts of the dataset between GPUs and the main memory [16]. Another possible solution [38] comes from the deep neural network training. It only checkpoints key intermediate results during the forward propagation and recalculates the missing results on demand during the backpropagation. Implementing the checkpoint mechanism is another potential optimization for GNN training.
5. *Sampling techniques can significantly reduce the memory usage per batch, but their implementation is still inefficient.* The sampling techniques are effective under small batch sizes for both training and inference. With proper batch sizes, the accuracy

of the sample-based training can be close to the accuracy of the full-batch training. However, the current implementation of the sampling techniques in PyG brings considerable overheads when the batch size is small. Improving the efficiency of the sampling techniques is a potential optimization direction. The small sampled subgraphs cannot make full use of the computing power of the GPU either. How to improve the GPU utilization under small batch sizes is another problem to solve. One possible solution is to train multiple batches asynchronously on the same GPU and use the asynchronous stochastic gradient descent to speed up the converge.

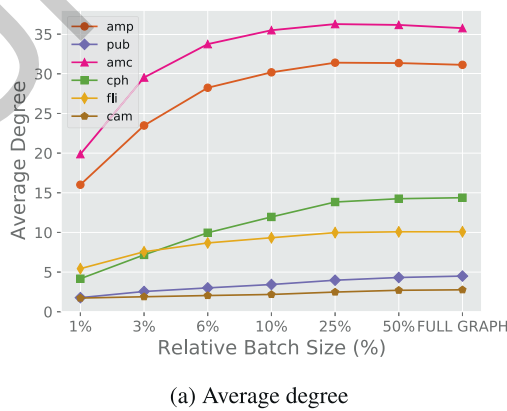
6. Related work

Survey of GNNs. Zhou et al. [8], Zhang et al. [9] and Wu et al. [10] survey the existing graph neural networks and classify them from an algorithmic view. They summarize the similarities and differences between the architectures of different GNNs. The typical applications of GNNs are also briefly introduced. Those surveys focus on comparing the existing GNNs theoretically, not empirically.

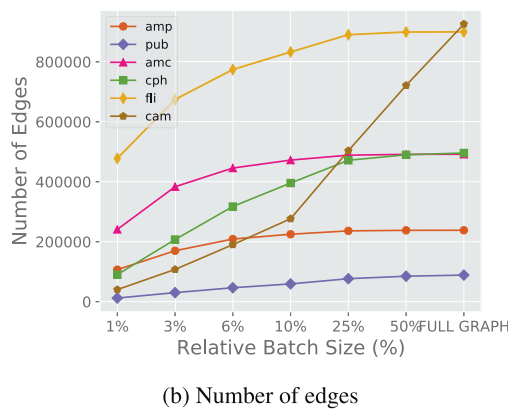
Evaluation of GNNs. Shchur et al. [33] evaluate the accuracy of popular GNNs on the node classification task. Dwivedi et al. [39] further compare the accuracy of popular GNNs fairly in a controlled environment. Hu et al. [40] propose the open graph benchmark that provides standard datasets and a standard evaluation workflow. The benchmark makes comparisons between GNNs easily and fairly. Those model evaluation efforts focus on evaluating the accuracy of different GNNs. They provide insightful suggestions to improve accuracy.

From the efficiency aspect, Yan et al. [19] compare the performance characteristics of graph convolutional networks, typical graph processing kernels (like PageRank), and the MLP-based neural networks on GPUs. They provide optimization guidelines for both the software and the hardware developers. Zhang et al. [20] analyze the architectural characteristics of the GNN inference on GPUs under SAGA-NN [16] model. They find that the GNN inference has no fixed performance bottleneck and all components deserve to optimize. These two efforts focus on the *inference* phase of GNNs and they investigate the potential optimizations mainly from an architectural view. In this work, our target is to find out the performance bottleneck in the training phase from a system view. We consider the performance bottleneck in both time and memory usage. We also evaluate the effects of the sampling techniques. Our work and the related evaluation [19,20] form a complementary study on the efficiency issue of GNNs.

Libraries/Systems for GNNs. PyG [14] and DGL [15] both adopt the message-passing framework as the underlying programming



(a) Average degree



(b) Number of edges

Fig. 35. Sizes of sampled subgraphs produced by the inference sampler under different relative batch sizes.

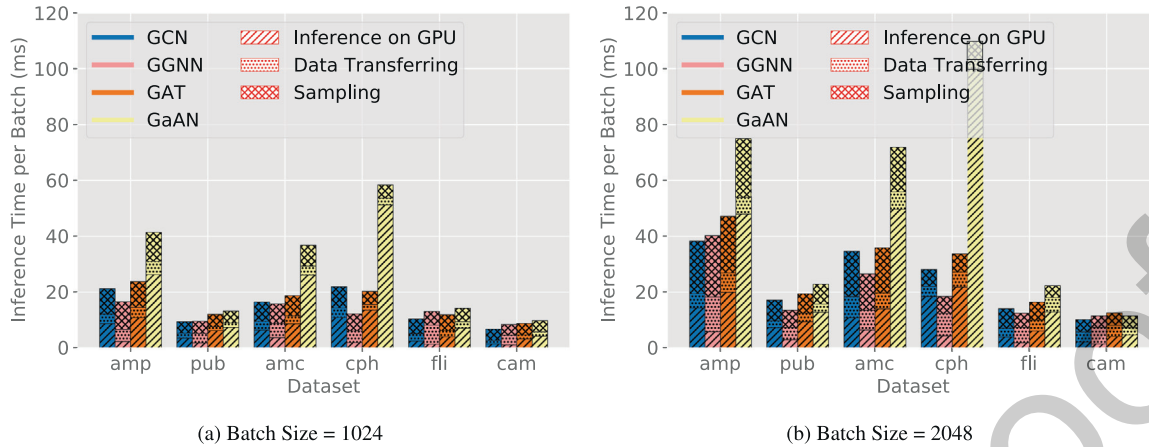


Fig. 36. Inference time per batch breakdown under different batch sizes.

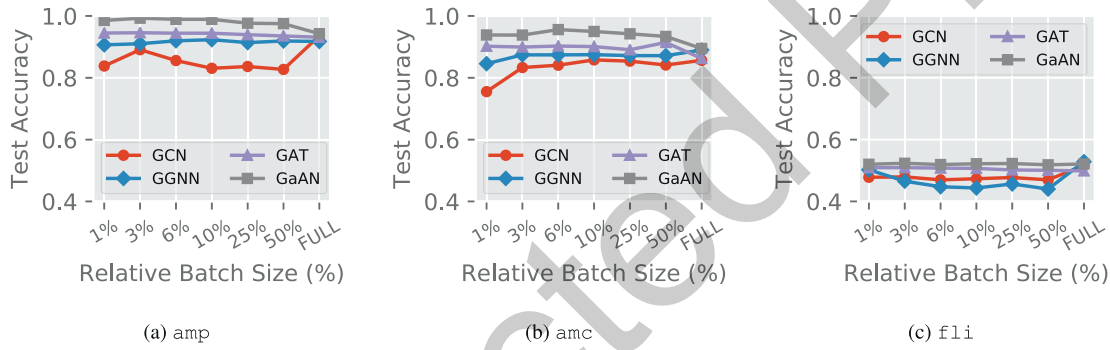


Fig. 37. Test accuracy under different batch sizes of the neighbor sampler. FULL means that the full graph participated in the training.

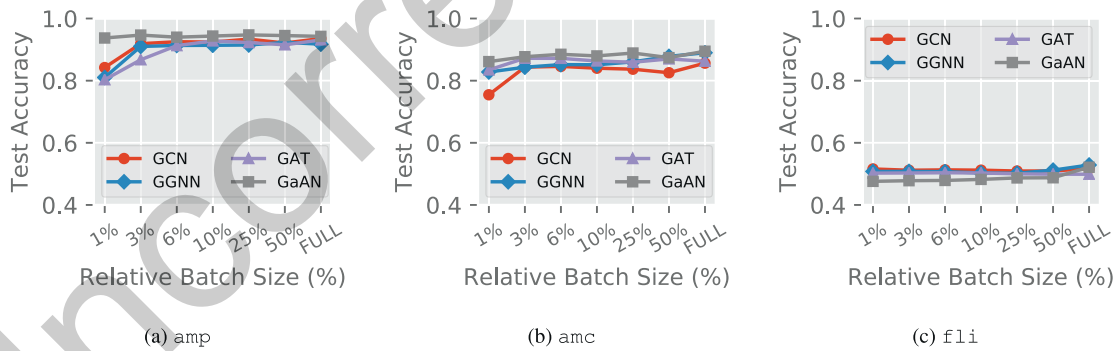


Fig. 38. Test accuracy under different batch sizes of the cluster sampler. FULL means that the full graph participated in the training.

model for GNNs and support training big datasets with the sampling techniques. PyG [14] is built upon PyTorch and it uses optimized CUDA kernels for GNNs to achieve high performance. DGL [15] provides a group of high-level user APIs and supports training GNNs with a variety of backends (TensorFlow, MXNet, and PyTorch) transparently. It also supports LSTM as the aggregation functions. NeuGraph [16] proposes a new programming model SAGA-NN for GNNs. It focuses on training big datasets efficiently without sampling. It partitions the dataset sophisticatedly, schedules the training tasks among multiple GPUs, and swaps the data among GPUs and the host asynchronously. AliGraph [17] targets at training GNNs on big attributed heterogeneous graphs that are common in e-commerce platforms. The graphs are partitioned

among multiple nodes in a cluster and AliGraph trains GNNs on the graphs in a distributed way with system optimizations. PGL [18] is another graph learning framework from Baidu based on the PaddlePaddle platform.

7. Conclusion and future work

In this work, we systematically explore the performance bottlenecks in graph neural network training and inference. We model the existing GNNs with the message-passing framework. We classify the GNNs according to their edge and vertex calculation complexity to select four typical GNNs for evaluation. The experimental results validate our complexity analysis. Fixing other hyper-

1268
1269
1270
1271
1272
1273
1274
1275
1276
1277
1278
1279
1280
1281
1282
1283
1284
1285
1286
1287
1288
1289
1290
1291

Z. Wang, Y. Wang, C. Yuan et al.

Neurocomputing xxx (xxxx) xxx

parameters, the training time, inference time, and memory usage increase linearly with each hyper-parameter of the four GNNs. To find out the performance bottlenecks in the training/inference time, we decompose the training/inference time per epoch on different levels. The time breakdown analysis indicates that the edge calculation stage and its related basic operators are the performance bottlenecks for most GNNs. Moreover, the intermediate results produced by the edge calculation stage cause high memory usage, limiting the data scalability. Adopting sampling techniques can reduce the memory usage of training and inference significantly, without sacrificing accuracy. However, the current implementation of the sampling techniques in PyG brings considerable sampling overheads. The small sampled subgraphs cannot make full use of the computing power of a GPU card either. Our analysis indicates that the edge calculation stage should be the main target of optimizations. Reducing its memory usage and improving its efficiency can significantly improve the performance of GNN training and inference. Based on the analysis, we propose several potential optimizations for the GNN libraries/systems. We believe that our analysis can help developers to have a better understanding of the characteristics of GNN training and inference.

Future Work. Specifically, in this work, we mainly analyze performance bottlenecks of GNN training/inference in the single-GPU environment on static graphs with the message-passing framework. In fact, performance bottlenecks of GNN training/inference over the multi-GPU or distributed environment, dynamic graphs, and other GNN frameworks are also worth studying. In the future, we plan to explore the GNN training/inference performance analysis under the following scenarios:

1. **Multi-GPU or distributed GNN training/inference.** To handle large-scale graph datasets, training/inferring GNNs with the multi-GPU environment or the distributed environment is essential. Multi-GPU and distributed GNN training/inference will inevitably introduce overheads such as inter-GPU and inter-machine communication. How these overheads affect performance bottlenecks is worthy to study.
2. **Spatial-temporal graph datasets.** Spatial-temporal graphs usually have dynamic topology structures. They appear in a variety of applications like traffic speed forecasting [41] and human action recognition [42]. Many new GNNs are proposed to handle this kind of dynamic graphs. The differences of performance issues between these GNNs and the classic GNNs are also worthy of in-depth investigation.
3. **Emerging GNN frameworks.** In this work, we analyzed the widely-used message-passing framework in GNN learning systems. However, some emerging GNN learning systems adopt different frameworks like the SAGA framework [16]. It is interesting to research whether different frameworks would lead to different performance bottlenecks.

CRediT authorship contribution statement

Zhaokang Wang: Conceptualization, Methodology, Investigation, Writing - original draft, Writing - review & editing. **Yunpan Wang:** Methodology, Software, Investigation, Writing - original draft, Writing - review & editing. **Chunfeng Yuan:** Writing - original draft. **Rong Gu:** Investigation, Writing - original draft, Writing - review & editing, Project administration, Funding acquisition. **Yihua Huang:** Conceptualization, Supervision, Funding acquisition.

Declaration of Competing Interest

The authors declare that they have no known competing financial interests or personal relationships that could have appeared to influence the work reported in this paper.

Acknowledgements

This work is funded in part by the National Key R&D Program of China (2019YFC1711000), the China NSF Grants (No. U1811461, 62072230), the Collaborative Innovation Center of Novel Software Technology and Industrialization, Jiangsu, China, Alibaba Innovative Research Project, and the program B for outstanding PhD candidate of Nanjing University.

References

- [1] T.N. Kipf, M. Welling, Semi-supervised classification with graph convolutional networks, in: Proceedings of the 5th International Conference on Learning Representations, 2017. URL: <https://openreview.net/forum?id=SlU4ayYgI>.
- [2] M. Defferrard, X. Bresson, P. Vandergheynst, Convolutional neural networks on graphs with fast localized spectral filtering, in: Advances in Neural Information Processing Systems, Vol. 29, Curran Associates Inc, 2016. URL: <https://proceedings.neurips.cc/paper/2016/hash/04df4d434d481c5bb723be1b6df1ee65-Abstract.html>.
- [3] R. Li, S. Wang, F. Zhu, J. Huang, Adaptive graph convolutional neural networks, in: Proceedings of the 32nd AAAI Conference on Artificial Intelligence AAAI, 2018, pp. 3546–3553. URL: <https://www.aaai.org/ocs/index.php/AAAI/AAI18/paper/view/16642>.
- [4] Y. Li, D. Tarlow, M. Brockschmidt, R.S. Zemel, Gated graph sequence neural networks, in: Proceedings of the 4th International Conference on Learning Representations ICLR, 2016, URL: <http://arxiv.org/abs/1511.05493>.
- [5] W.L. Hamilton, Z. Ying, J. Leskovec, Inductive representation learning on large graphs, in: Advances in Neural Information Processing Systems, Vol. 30, Curran Associates Inc, 2017. URL: <https://proceedings.neurips.cc/paper/2017/hash/5dd9db5e033da9c6fb5ba83c7a7ebea9-Abstract.html>.
- [6] P. Velickovic, G. Cucurull, A. Casanova, A. Romero, P. Liò, Y. Bengio, Graph attention networks, in: Proceedings of the 6th International Conference on Learning Representations, 2018, URL: <https://openreview.net/forum?id=rJXMpikCZ>.
- [7] J. Zhang, X. Shi, J. Xie, H. Ma, I. King, D. Yeung, Gaan: Gated attention networks for learning on large and spatiotemporal graphs, in: Proceedings of the 34th Conference on Uncertainty in Artificial Intelligence, AUAI Press, 2018, pp. 339–349, URL: <http://auai.org/uai2018/proceedings/papers/139.pdf>.
- [8] J. Zhou, G. Cui, Z. Zhang, C. Yang, Z. Liu, L. Wang, C. Li, M. Sun, Graph neural networks: A review of methods and applications, URL: <https://arxiv.org/abs/1812.08434> (2018).
- [9] Z. Zhang, P. Cui, W. Zhu, Deep learning on graphs: A survey, IEEE Trans. Knowl. Data Eng. (Early Access) (2020) 1, <https://doi.org/10.1109/TKDE.2020.2981333>.
- [10] Z. Wu, S. Pan, F. Chen, G. Long, C. Zhang, P.S. Yu, A comprehensive survey on graph neural networks, IEEE Trans. Neu. Netw. Learn. Syst. 32 (1) (2021) 4–24, <https://doi.org/10.1109/TNNLS.2020.2978386>.
- [11] S. Qi, W. Wang, B. Jia, J. Shen, S. Zhu, Learning human-object interactions by graph parsing neural networks, in: V. Ferrari, M. Hebert, C. Sminchisescu, Y. Weiss (Eds.), Proceedings of the European Conference on Computer Vision (ECCV), Vol. 11213 of Lecture Notes in Computer Science Springer, 2018, pp. 407–423, https://doi.org/10.1007/978-3-030-01240-3_25.
- [12] W. Wang, H. Zhu, J. Dai, Y. Pang, J. Shen, L. Shao, Hierarchical human parsing with typed part-relation reasoning, in, in: Proceedings of the 2020 IEEE/CVF Conference on Computer Vision and Pattern Recognition IEEE, 2020, pp. 8926–8936, <https://doi.org/10.1109/CVPR42600.2020.00895>.
- [13] W. Wang, X. Lu, J. Shen, D.J. Crandall, L. Shao, Zero-shot video object segmentation via attentive graph neural networks, in: Proceedings of the 2019 IEEE/CVF International Conference on Computer Vision IEEE, 2019, pp. 9235–9244, <https://doi.org/10.1109/ICCV.2019.00933>.
- [14] M. Fey, J.E. Lenssen, Fast graph representation learning with pytorch geometric, URL: <https://arxiv.org/abs/1903.02428> (2019).
- [15] M. Wang, L. Yu, D. Zheng, Q. Gan, Y. Gai, Z. Ye, M. Li, J. Zhou, Q. Huang, C. Ma, Z. Huang, Q. Guo, H. Zhang, H. Lin, J. Zhao, J. Li, A.J. Smola, Z. Zhang, Deep graph library: Towards efficient and scalable deep learning on graphs, URL: <https://arxiv.org/abs/1909.01315v1> (2019).
- [16] L. Ma, Z. Yang, Y. Miao, J. Xue, M. Wu, L. Zhou, Y. Dai, Neugraph: Parallel deep neural network computation on large graphs, in: Proceedings of the 2019 USENIX Annual Technical Conference, USENIX Association, 2019, pp. 443–458. URL: <https://www.usenix.org/conference/atc19/presentation/ma>.
- [17] R. Zhu, K. Zhao, H. Yang, W. Lin, C. Zhou, B. Ai, Y. Li, J. Zhou, Alignraph: A comprehensive graph neural network platform, Proceedings of the VLDB Endowment 12 (12) (2019) 2094–2105, <https://doi.org/10.14778/3352063.3352127>.
- [18] Baidu, Paddle graph learning, URL: <https://github.com/PaddlePaddle/PGL>.
- [19] M. Yan, Z. Chen, L. Deng, X. Ye, Z. Zhang, D. Fan, Y. Xie, Characterizing and understanding GCNs on GPU, IEEE Comput. Arch. Lett. 19 (1) (2020) 22–25, <https://doi.org/10.1109/LCA.2020.2970395>.
- [20] Z. Zhang, J. Leng, L. Ma, Y. Miao, C. Li, M. Guo, Architectural implications of graph neural networks, IEEE Comput. Arch. Lett. 19 (1) (2020) 59–62, <https://doi.org/10.1109/LCA.2020.2988991>.

Z. Wang, Y. Wang, C. Yuan et al.

Neurocomputing xxx (xxxx) xxx

- [21] B. Perozzi, R. Al-Rfou, S. Skiena, Deepwalk: online learning of social representations, in: Proceedings of the 20th ACM SIGKDD International Conference on Knowledge Discovery and Data Mining ACM, 2014, pp. 701–710, <https://doi.org/10.1145/2623330.2623732>.
- [22] A. Grover, J. Leskovec, node2vec: Scalable feature learning for networks, in: Proceedings of the 22nd ACM SIGKDD International Conference on Knowledge Discovery and Data Mining ACM, 2016, pp. 855–864, <https://doi.org/10.1145/2939672.2939754>.
- [23] J. Gilmer, S.S. Schoenholz, P.F. Riley, O. Vinyals, G.E. Dahl, Neural message passing for quantum chemistry, in: Proceedings of the 34th International Conference on Machine Learning, Vol. 70, PMLR, 2017, pp. 1263–1272. URL: <http://proceedings.mlr.press/v70/gilmer17a.html>.
- [24] D.K. Duvenaud, D. Maclaurin, J. Iparragirre, R. Bombarell, T. Hirzel, A. Aspuru-Guzik, R.P. Adams, Convolutional networks on graphs for learning molecular fingerprints, in: Advances in Neural Information Processing Systems, Vol. 28, Curran Associates Inc, 2015. URL: <https://proceedings.neurips.cc/paper/2015/hash/f9be311e65d81a9ad8150a60844b94c-Abstract.html>.
- [25] H. Dai, Z. Kozareva, B. Dai, A.J. Smola, L. Song, Learning steady-states of iterative algorithms over graphs, in: Proceedings of the 35th International Conference on Machine Learning, Vol. 80, PMLR, 2018, pp. 1114–1122. URL: <http://proceedings.mlr.press/v80/dai18a.html>.
- [26] W.-L. Chiang, X. Liu, S. Si, Y. Li, S. Bengio, C.-J. Hsieh, Cluster-GCN: An efficient algorithm for training deep and large graph convolutional networks, in: Proceedings of the 25th ACM SIGKDD International Conference on Knowledge Discovery and Data Mining ACM, 2019, pp. 257–266, <https://doi.org/10.1145/3292500.3330925>.
- [27] R. Ying, R. He, K. Chen, P. Eksombatchai, W.L. Hamilton, J. Leskovec, Graph convolutional neural networks for web-scale recommender systems, in: Proceedings of the 24th ACM SIGKDD International Conference on Knowledge Discovery and Data Mining ACM, 2018, pp. 974–983, <https://doi.org/10.1145/3219819.3219890>.
- [28] J. Chen, T. Ma, C. Xiao, FastGCN: Fast learning with graph convolutional networks via importance sampling, in: Preceedings of the 6th International Conference on Learning Representations, 2018, URL: <https://openreview.net/forum?id=rytstxWWA>.
- [29] J. Chen, J. Zhu, L. Song, Stochastic training of graph convolutional networks with variance reduction, in: Proceedings of the 35th International Conference on Machine Learning, Vol. 80, PMLR, 2018, pp. 942–950. URL: <http://proceedings.mlr.press/v80/chen18p.html>.
- [30] H. Zeng, H. Zhou, A. Srivastava, R. Kannan, V.K. Prasanna, Accurate, efficient and scalable graph embedding, in: Proceedings of the 2019 IEEE International Parallel and Distributed Processing Symposium IEEE, 2019, pp. 462–471, <https://doi.org/10.1109/IPDPS.2019.00056>.
- [31] H. Zeng, H. Zhou, A. Srivastava, R. Kannan, V.K. Prasanna, Graphsaint: Graph sampling based inductive learning method, in: Proceedings of the 8th International Conference on Learning Representations, 2020, URL: <https://openreview.net/forum?id=Bje8pkHFWS>.
- [32] W. Huang, T. Zhang, Y. Rong, J. Huang, Adaptive sampling towards fast graph representation learning, in: Advances in Neural Information Processing Systems, Vol. 31, Curran Associates Inc, 2018. URL: <https://proceedings.neurips.cc/paper/2018/hash/01eee509ee2f68dc6014898c309e86bf-Abstract.html>.
- [33] O. Shchur, M. Mumme, A. Bojchevski, S. Günnemann, Pitfalls of graph neural network evaluation, URL: <http://arxiv.org/abs/1811.05868> (2018).
- [34] J. Yang, J. Leskovec, Defining and evaluating network communities based on ground-truth, in: Proceedings of the 12th IEEE International Conference on Data Mining IEEE, 2012, pp. 745–754, <https://doi.org/10.1109/ICDM.2012.138>.
- [35] D. Chakrabarti, Y. Zhan, C. Faloutsos, R-mat: A recursive model for graph mining, Proceedings of the 2004 SIAM International Conference on Data Mining, pp. 442–446, <https://doi.org/10.1137/1.9781611972740.43>.
- [36] D.P. Kingma, J. Ba, Adam: A method for stochastic optimization, in: Proceedings of the 3rd International Conference on Learning Representations, 2015, URL: <http://arxiv.org/abs/1412.6980>.
- [37] X. Glorot, Y. Bengio, Understanding the difficulty of training deep feedforward neural networks, in: Proceedings of the Thirteenth International Conference on Artificial Intelligence and Statistics, Vol. 9, JMLR Workshop and Conference Proceedings, 2010, pp. 249–256. URL: <https://proceedings.mlr.press/v9/glorot10a.html>.
- [38] T. Chen, B. Xu, C. Zhang, C. Guestrin, Training deep nets with sublinear memory cost, URL: <https://arxiv.org/abs/1604.06174> (2016).
- [39] V.P. Dwivedi, C.K. Joshi, T. Laurent, Y. Bengio, X. Bresson, Benchmarking graph neural networks, URL: <https://arxiv.org/abs/2003.00982> (2020).
- [40] W. Hu, M. Fey, M. Zitnik, Y. Dong, H. Ren, B. Liu, M. Catasta, J. Leskovec, Open graph benchmark: Datasets for machine learning on graphs, in: Advances in Neural Information Processing Systems, Vol. 33, Curran Associates Inc, 2020. URL: <https://proceedings.neurips.cc/paper/2020/hash/fb60d411a5c5b72b2e7d3527fc84fd0-Abstract.html>.
- [41] Y. Li, R. Yu, C. Shahabi, Y. Liu, Diffusion convolutional recurrent neural network: Data-driven traffic forecasting, in: Proceedings of the 6th International Conference on Learning Representations, 2018, URL: <https://openreview.net/forum?id=SjHXGWAZ>.
- [42] S. Yan, Y. Xiong, D. Lin, Spatial temporal graph convolutional networks for skeleton-based action recognition, in: in: Proceedings of the 32nd AAAI Conference on Artificial Intelligence AAAI, 2018, pp. 7444–7452, URL: <https://www.aaai.org/ocs/index.php/AAAI/AAAI18/paper/view/17135>.

Zhaokang Wang received the BS degree in Nanjing University, China, in 2013. He is currently working towards the Ph.D. degree in Nanjing University. His research interests include large scale graph analysis algorithms and graph processing systems.



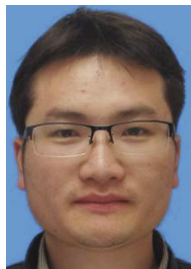
Yunpan Wang received the BS degree in University of Electronic Science and Technology of China in 2018. He is currently working towards the master degree in Nanjing University. His research interests include distributed deep learning, graph computing systems.



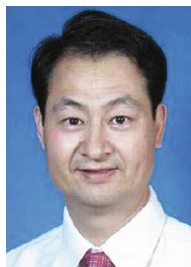
Chunfeng Yuan is currently a professor in the computer science department and State Key Laboratory for Novel Software Technology, Nanjing University, China. She received her bachelor and master degrees in computer science from Nanjing University. Her main research interests include computer architecture, parallel and distributed computing and information retrieval.



Rong Gu is an associate researcher at State Key Laboratory for Novel Software Technology, Nanjing University, China. Dr. Gu received the Ph.D. degree in computer science from Nanjing University in December 2016. His research interests include parallel computing, distributed systems and distributed machine learning.



Yihua Huang is currently a professor in computer science department and State Key Laboratory for Novel Software Technology, Nanjing University, China. He received his bachelor, master and Ph.D. degrees in computer science from Nanjing University. His main research interests include parallel and distributed computing, big data parallel processing, distributed machine learning algorithm and system, and Web information mining.



1516
1520
1521
1522
1523
1524

1518
1527
1528
1529
1530
1531
1532

1526
1535
1536
1537
1538
1539
1540
1541
1542

1534
1545
1546
1547
1548
1549
1550
1551

1544
1554
1555
1556
1557
1558
1559
1560
1561
1562
1563

1553